

Was there a volcanic induced long lasting cooling over the Northern Hemisphere in the mid 6th-7th century?

Evelien van Dijk¹, Johann Jungclaus², Stephan Lorenz², Claudia Timmreck², and Kirstin Krüger¹

¹Department of Geosciences, University of Oslo, Oslo, Norway

²Max Planck Institute for Meteorology, Hamburg, Germany

Correspondence: Evelien van Dijk (evelien.van.dijk@geo.uio.no) and Kirstin Krüger (kirstin.krueger@geo.uio.no)

Abstract. The climate in the Northern Hemisphere (NH) of the mid-6th century was one of the coldest during the last two millennia based on multiple paleo-proxies. While the onset of this cold period can be clearly connected to the volcanic eruptions in 536 and 540 Common Era (CE), the duration, extent and magnitude of the cold period is uncertain. Proxy data are sparse for the first millennium, which exacerbates the uncertainties of the reconstructions. To better understand the mechanisms of the 5 prolonged cooling, we analyze new transient simulations over the Common Era and enhance the representation of mid 6th to 7th century climate by additional ensemble simulations covering 520-680 CE. We use the Max Planck Institute Earth System Model and apply the external forcing as recommended in the Paleo Model Intercomparison Project, Phase 4.

After the four large eruptions in 536, 540, 574 and 626 CE, a significant surface climate response in the NH lasting up to 20 years is simulated. The 2m air temperature shows a cooling over the Arctic in winter, corresponding to the increase in 10 Arctic sea-ice, mainly in the Labrador sea and east of Greenland. The increase in sea-ice extent is related to a decrease in the northward ocean heat transport into the Arctic in the first two years after the eruptions and to an increase in the Atlantic Meridional Overturning Circulation, which peaks 10 years after the eruptions. A decrease in the global ocean heat content is simulated after the eruptions that does not recover for the entire simulation period. These ocean – sea-ice interactions sustain the surface cooling, as the cooling lasts longer as is expected solely from the direct effects of the volcanic forcing, 15 and are thus responsible for the multidecadal surface cooling. In boreal summer, the main cooling occurs over the continents at mid-latitudes. A dipole pattern develops with high sea level pressure and a decrease in both precipitation and evaporation poleward of 40°N. In addition, a land-sea contrast with decreased values over land and an increase in values over the ocean occurs. While our model ensemble simulations show a similar ~ 20 year summer cooling over NH land after the eruptions as 20 ensemble reconstructions from tree-ring width data, a volcanic induced century long surface cooling as derived for some tree ring sites does not occur in our simulations.

1 Introduction

Large volcanic eruptions are the major driver of natural climate variability in the pre-industrial era of the last millennium (Hegerl et al., 2006; Schurer et al., 2014). In order to assess what potential impact they could have on future climate, it is

important to understand what the climate response to volcanic forcing was in the past, and which mechanisms are involved.

25

Several cluster eruptions and double eruption events occurred in the last 2000 years, coinciding with cold periods in Northern Hemisphere (NH) tree-ring records (Briffa et al., 1998; Sigl et al., 2013). One of the coldest decades of the last 2000 years in Europe and the NH is visible in tree-ring records during the mid-sixth century (e.g., Larsen et al., 2008; Büntgen et al., 2011; Sigl et al., 2015). Historic documents report a dimming of the sun in 536 CE (Stothers, 1984; Rampino et al., 1988), and a shift in ice-core records lead to the two volcanic peaks to correspond to the 536 and 540 CE eruptions (Baillie, 2008; Sigl et al., 2015). Reconstructed tree-ring temperatures from the Alps and Altai show a century-long cooling that might have exceeded that of the Little Ice Age (LIA) during the 14th-19th century (Büntgen et al., 2016). Thus, this period was called the Late Antiquity Little Ice Age (LALIA). However, other proxies, including tree-ring, ice-core and documentary evidence, from the NH extratropics only indicate a multi-decadal cooling until ~570 CE rather than a centennial one (Helama et al., 2017). This all lines up to a cold period that was initiated by volcanic eruptions. Indeed, four large volcanic eruptions occurred in 536, 540, 574, and 626 CE (Sigl et al., 2015).

Climate models can shed light on not only the climate response, but also on the underlying mechanisms and feedbacks. With the help of climate models we can test if a series of volcanic eruptions may have caused severe long-lasting cooling over the NH and Europe during the mid 6th to 7th century. Previous model studies have simulated the surface climate response to volcanic eruptions in the last millennium, and found up to a decade of surface cooling due to extremely large eruptions (Stenchikov et al., 2009; Timmreck et al., 2009). Others show that the LIA could have been triggered by volcanic eruptions (Schneider et al., 2009; Miller et al., 2012). If consecutive eruptions occur within a few years, sea ice-ocean feedback mechanisms may maintain the surface cooling over longer time scales, from years to decades (Myhre et al., 2013). A series of decadally-paced volcanic eruptions in the mid 13th century has been suggested to have caused the onset of the LIA (Zhong et al., 2011; Miller et al., 2012) and ocean - sea-ice feedbacks have been connected to this cooling (Lehner et al., 2013; Moreno-Chamarro et al., 2017). However, hardly any modeling studies investigating volcanic-climate impacts during the first millennium exist. Toohey et al. (2016a) carried out climate simulations from 536-550 CE, analyzing the effect of the 536/540 CE volcanic double event on the NH surface climate. The volcanic forcing was reconstructed based on the sulfate deposition in ice cores and the aerosol climate model MAECHAM-HAM (see Table 1), which was used as input for the Max Planck Institute Earth System Model (MPI-ESM) climate simulations. They found decreased NH temperature anomalies of maximum 2°C and increased Arctic sea-ice after the volcanic double event lasting the entire simulation period of 15 years. However, this simulation period was too short to study multidecadal cooling, as has been reconstructed (Büntgen et al., 2016; Helama et al., 2017), and were started from a pre-industrial conditions control run.

55

The aim of this study is to investigate whether a series of volcanic eruptions induced a multidecadal to centennial cooling in the mid 6th to 7th century. We performed 160 year long (520-680 CE) MPI-ESM ensemble simulations branched off one Paleoclimate Modeling Intercomparison Project phase 4 (PMIP4) past2k simulation (Jungclaus et al., 2017). We focus

in particular on the NH and European climate in comparison with available temperature proxy reconstructions. Multiproxy
60 reconstructions in the NH during this period consist of mainly tree-ring, marine sediments, and ice core records. Marine sediments have a coarse chronological resolution and would therefore not capture the volcanic signal, and ice core records are confined to the Greenland Ice-sheet (Consortium et al., 2017, 2017). Tree-ring records have an annual resolution with an absolute dating. Therefore, we use the most recent tree ring ensemble reconstruction for the past2k (Büntgen et al., 2021) to compare to the model simulations in this study. In contrast to the study of Toohey et al. (2016a), the short term (annual), as
65 well as the long term (decadal to centennial) effects of the 536/540 CE volcanic double event plus the other eruptions during 520-680 CE on the coupled climate system are analyzed. In addition to the surface climate and sea ice impacts, we also study changes in atmospheric and ocean circulation, hydrology and ocean-sea ice feedbacks, processes important in maintaining the volcanic induced surface cooling.

In Section 2, the model details, set up and experiments, as well as tree-ring data are described. In Section 3, the model results
70 are presented and discussed. Finally, a summary and conclusion are given in Section 4.

2 Methods

Model and experiment description

The MPI-ESM model

The MPI-ESM1.2.01p5 taken for this study is the low-resolution (LR) version used for the Coupled Model Intercomparison
75 Project phase 6 (CMIP6) and the PMIP4. The atmosphere component (ECHAM6.3, Stevens et al., 2013) has a horizontal resolution of $1.9^\circ \times 1.9^\circ$ and 47 vertical layers (T63L47) up to 0.01 hPa or 80 km altitude. The ocean component (MPIOM 1.6 GR1.5/L40, Jungclaus et al., 2013) features a conformal mapping grid with a nominal resolution of 1.5° . The grid poles are placed over Greenland and Antarctica and the actual horizontal resolution ranges from 22 km near Greenland to roughly 200 km in the Pacific Ocean. The vertical grid is represented on 40 unevenly spaced z-levels, with 20 levels in the upper 700
80 m. A complete description of MPI-ESM1.2 in its CMIP6 configurations, including parameter and tuning choices, is given by Mauritsen et al. (2019).

The PMIP4 - past2k simulations

For its fourth phase, PMIP has selected four experiments as contribution to CMIP6 (Kageyama et al., 2017). In addition to time-slice experiments, the transient simulation over the last millennium “past1000” was chosen as a core experiment.
85 The “past1000” experimental protocol (Jungclaus et al., 2017) describes several extensions to the standard last millennium simulation and includes the tier-3-category “past2k” experiment that covers the entire CE. The aim of the “past2k” experiment is to extend the scope of the PMIP transient simulations further back into the past and to encourage model-data comparison studies taking full advantage of the past global changes (PAGES) “PAST2K” data base (Martrat et al., 2019). The MPI-ESM experiments described here are, to our knowledge, the first past2k runs that are fully compliant with the CMIP6 and PMIP4

90 protocols. The two simulations started from different dates taken from the end of a 1200-year long “spin-down” simulation under constant 1 CE boundary conditions, which was initialized from the MPI-ESM-LR piControl simulation for CMIP6. Only one of these simulations included all the output options necessary to produce CMOR-compliant output (Eyring et al., 2016) for publication on the Earth System Grid Federation (ESGF). This past2k run is referred to as past2k “run 1” from here on, and the other past2k run is referred to as past2k “run 0”.

95 **The 520-680 CE simulations**

For this study, we ran ten ensemble members, covering the period 520-680 CE. The simulations are branched off one of the two past2k runs (run 0) in the year 521 by perturbing the climate. For each ensemble member the atmospheric diffusivity was changed by $1 \cdot 10^{-5} \text{ m}^2 \text{s}^{-1}$ to simulate slightly different climate states by the year 536 CE, the year of the first large volcanic eruption. In contrast to other studies, where the initial state was simply taken from a pre-industrial control simulation, 100 our approach allows us to include the climate and forcing history of the previous decades and centuries as well as their integrative effects (Gleckler et al., 2006). The simulations were run with the new volcanic forcing for PMIP4, as well as best estimate conditions for the 6th-7th century (see external forcing section). For the ensemble mean results (n=12), we included ten ensemble members from the 520-680 CE and two ensemble members from the PMIP4 past2k simulations. The anomalies were calculated by subtracting the mean of 0-1850 CE from the past2k “run 0” from the mean of the volcanic ensemble. We 105 use the average over 0-1850 CE to have a reference climate that is representative for the entire pre-industrial Common Era. We tested also different anomaly calculations with a reference period 10 years before the 536 CE eruption, as well as 1200 years of the control run, both without volcanic eruptions, and the resulting temperature anomalies are within +/- 0.15 K. The significance was calculated from the 1200 year control run. To account for the different response times of 2 and 20 years, the 2 and 20 year means were taken from the 1200 year control run. As the mean response is for 4 eruptions, 4 random time steps 110 were taken from the mean control time series to account for this. To get a significant sample, this was iterated 1000 times for each variable, and from these 1000 samples a new time series was created. The standard deviation was then calculated from this random time series. 1 or 2 sigma were calculated for the significance levels.

External forcing

The external forcing for the MPI-ESM simulations follows the protocol by Jungclaus et al. (2017) using the respective default 115 choices for the past1000 experiment. Except for land-use/land-cover change data, all external forcing agents described in Jungclaus et al. (2017), see below, are available for the entire CE. Total solar irradiance and spectral solar irradiance are derived from cosmogenic radio isotopes through a chain of physics-based models (Vieira et al., 2011; Usoskin et al., 2014), and we chose here the 14C-based SATIRE-M version (see Section 3). The effect of solar-derived ozone changes is parameterized by a simple scaling scheme. Greenhouse gases ($\text{CO}_2, \text{CH}_4, \text{N}_2\text{O}$) follow the recommendations for CMIP6 (Meinshausen 120 et al., 2016), and the orbital parameters are calculated internally in ECHAM6’s calendar routine. The CMIP6 land-use and anthropogenic land-cover changes have been reconstructed for the period 850 to 2014 CE (Jungclaus et al., 2017; Hurt et al., 2020). The data set is based on modern estimates of division into several agricultural uses and urban areas coming from the

Historical Land Use Data Set for the Holocene (HYDE3.2, Klein Goldewijk, 2016). Considering several options (e.g. linear ramp-up) we prescribed a constant land-cover for the first 850 years of the past2k runs.

125 Volcanic forcing

The volcanic forcing used for the runs is described by Jungclaus et al. (2017) with details on the eVolv2k data set being described by Toohey and Sigl (2017). eVolv2k is used in combination with the Easy Volcanic Aerosol module (EVA), as described by Toohey et al. (2016b). The eVolv2k includes estimates of stratospheric sulfur injections (VSSI) and the locations of the eruptions (latitudes) based on ice core data from Antarctica and Greenland. A calibration factor is used to convert the 130 ice core deposition value to stratospheric sulfur loading (Gao et al., 2007). The details of the eruptions occurring in the period of the ensemble runs are given in Fig. 1. The eruptions are set to January in the model forcing as the actual eruption month is unknown. Each eruption gives an abrupt increase in aerosol optical depth (AOD), and the differences between them are distinct. In this study, we focus on the four largest eruptions out of the 14 in the study period, where 536 CE and 626 CE are 135 NH extra-tropical eruptions and 540 CE and 574 CE eruptions are tropical eruptions (Table 1). For the NH extra-tropical eruptions, the aerosols are mainly contained within the NH hemisphere, whereas for the tropical eruptions the AOD spreads out over both hemispheres. Figure 1b shows the accumulated AOD per latitude for 15 year intervals, where 535-550 CE stands out as the period with the strongest forcing of the 160-year simulation period.

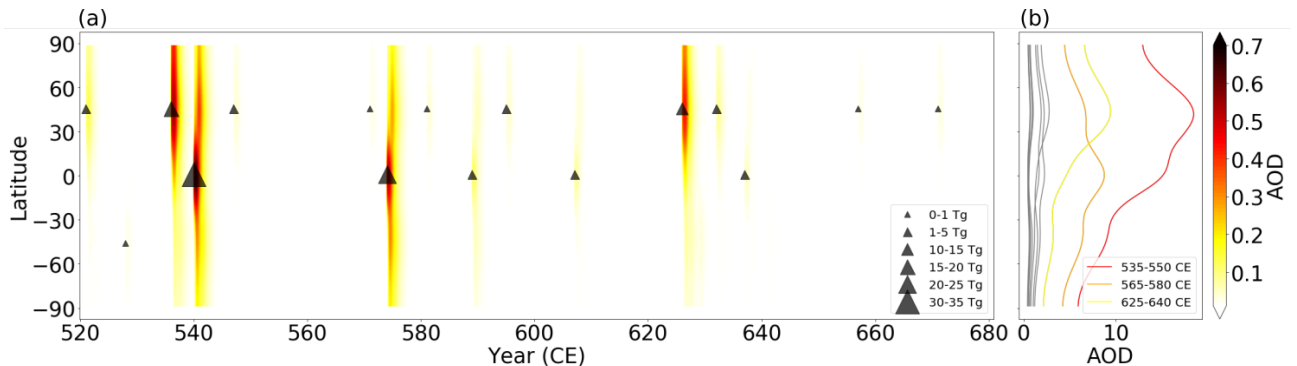


Figure 1. a) Zonal mean volcanic forcing (Aerosol Optical Depth, AOD) for the study period (520-680 CE) and b) zonal mean accumulated AOD (520-680 CE) in 15 year bins from the reconstructed volcanic forcing of Toohey and Sigl (2017). The three 15 year periods with the highest volcanic forcing are highlighted in color and labeled. The triangles in (a) highlight the zonal locations and different strength in terms of stratospheric sulfur injection of all volcanic eruptions as specified in the legend ($Tg = 10^{12} g$).

Table 1. Volcanic forcing and stratospheric sulfur injection for eruptions used in this study (based on eVolv2k; Toohey and Sigl, 2017). Details for the Toohey et al. (2016a) 536 and 540 CE reconstruction based on MAECHAM-HAM are added. The four, respectively, two largest eruptions are highlighted as bold text.

Eruption year	Eruption month	Eruption latitude	S [Tg]	Max global AOD	Reference
521	Jan	NH extratropical	3.7 Tg	0.07	Toohey and Sigl (2017)
528	Jan	SH extratropical	0.8 Tg	0.01	
536	Jan	NH extratropics	18.8	0.29	
540	Jan	Tropics	31.8	0.38	
547	Jan	NH extratropical	1.1 Tg	0.02	
571	Jan	NH extratropical	0.7 Tg	0.01	
574	Jan	Tropics	24.1	0.31	
581	Jan	NH extratropical	0.9 Tg	0.02	
589	Jan	Tropical	4.4 Tg	0.07	
595	Jan	NH extratropical	1.1 Tg	0.02	
607	Jan	Tropical extratropical	2.7 Tg	0.04	
626	Jan	NH extratropics	13.2	0.21	
632	Jan	NH extratropical	2.1 Tg	0.04	
637	Jan	Tropical	1.7 Tg	0.03	
657	Jan	NH extratropical	0.7 Tg	0.01	
671	Jan	NH extratropical	0.8 Tg	0.01	
536	March	42°N	15	0.9	Toohey et al. (2016a)
540	Jan	15°N	25	0.9	

Tree-ring data

For the model-tree-ring comparison, the tree-ring ensemble reconstruction from Büntgen et al. (2021) was used. The raw data is taken from 9 sites over the NH (Fig. A1), which has then been distributed to 15 different dendrochronology groups. These groups all carried out their own statistical methods on the data, after which the now different data sets were combined to form

a tree-ring ensemble. The data sets are based on tree ring width (TRW). TRW is known to have biological memory and gives a lagged and smoothed response to volcanic eruptions. However, the alternative, Maximum latewood density (MXD) data is sparse during the first millennium, and so the tree ring proxy ensemble reconstruction used here consist only of TRW data.

145 To use the same reference period for the model and tree-ring data, we subtracted the 0-1850 CE mean from the model and tree-ring ensemble. For the model-tree-ring comparison a land mask was applied to the model 2m air temperature and we analyzed only the NH extratropics between 40° and 75°N. The tree-ring data sets capture the boreal summer temperature during June, July and August (JJA) and were therefore compared to JJA 2m air temperatures from the model.

3 Results

150 Volcanic response

Figure 2 displays the evolution of NH 2m air temperature for the ensemble in comparison with the entire past2k simulations. The variations in the ensemble simulations fall within the variability of the past2k runs and the volcanic signals are significant and clearly stand out (Fig. 2a). The four large eruptions in the period 520-680 also clearly stand out in the yearly mean NH 2m air temperature, precipitation and sea-ice area anomalies and the ocean heat content for the upper 700 m (Figure 2). Variations 155 in the solar forcing are very small compared to the volcanic forcing and can not explain these distinct deviations. Following the 540 CE eruption, maximum deviations are reached during the 520-680 period, with a peak cooling of the NH 2m air temperature of ~ 2 K, precipitation decrease of 0.2 mm/day, ocean heat content decrease in the upper 700 m of $1.5 \cdot 10^{23} \text{ J m}^{-1}$, as well as an increase in the Arctic sea-ice area of $1.5 \cdot 10^{12} \text{ m}^2$ compared to the 0-1850 CE mean.

The responses in surface climate show a longer recovery than the AOD, indicating that additional processes play a role in 160 cooling the surface climate after volcanic eruptions. The AOD peaks after ~ 12 months and is back at 0 after 3-4 years (Fig. 2b). The temperature (Fig. 2c) reveals a maximum cooling in the first and second year after the eruption and is decreased for 20 years after the 540 CE, for 30 years after the 574 CE and for 14 years after 626 CE eruptions, much longer than the direct response of the AOD. The temperature decrease and sea-ice extent increase (Fig. 2e) peak simultaneously, and show a similar long recovery after the eruptions. The precipitation decrease follows a similar pattern as temperature and sea ice area 165 changes, but with a shorter recovery period. The precipitation anomalies are back to zero after 10-15 years after the eruptions. The global ocean heat content anomaly for the upper 700 m (Fig. 2f) shows a maximum decrease right after the eruptions, which is significant for 30-40 years, and it does not go back to 0 anomaly during the entire study period. The global ocean heat content is the only variable that reveals a century long anomaly due to the subsequent eruptions. The Atlantic ocean heat transport at 60°N reflects high inter-annual variability, which makes it hard to distinguish any significant volcanic signal. After 170 all large volcanic eruption we diagnose a robust decrease in northward heat transport, even though it rarely exceeds the 2-sigma threshold derived from the control simulation. (Fig. 2g). Towards the end of the simulation, period the ensemble shows a larger spread in the ocean heat content than at the beginning of the simulations.

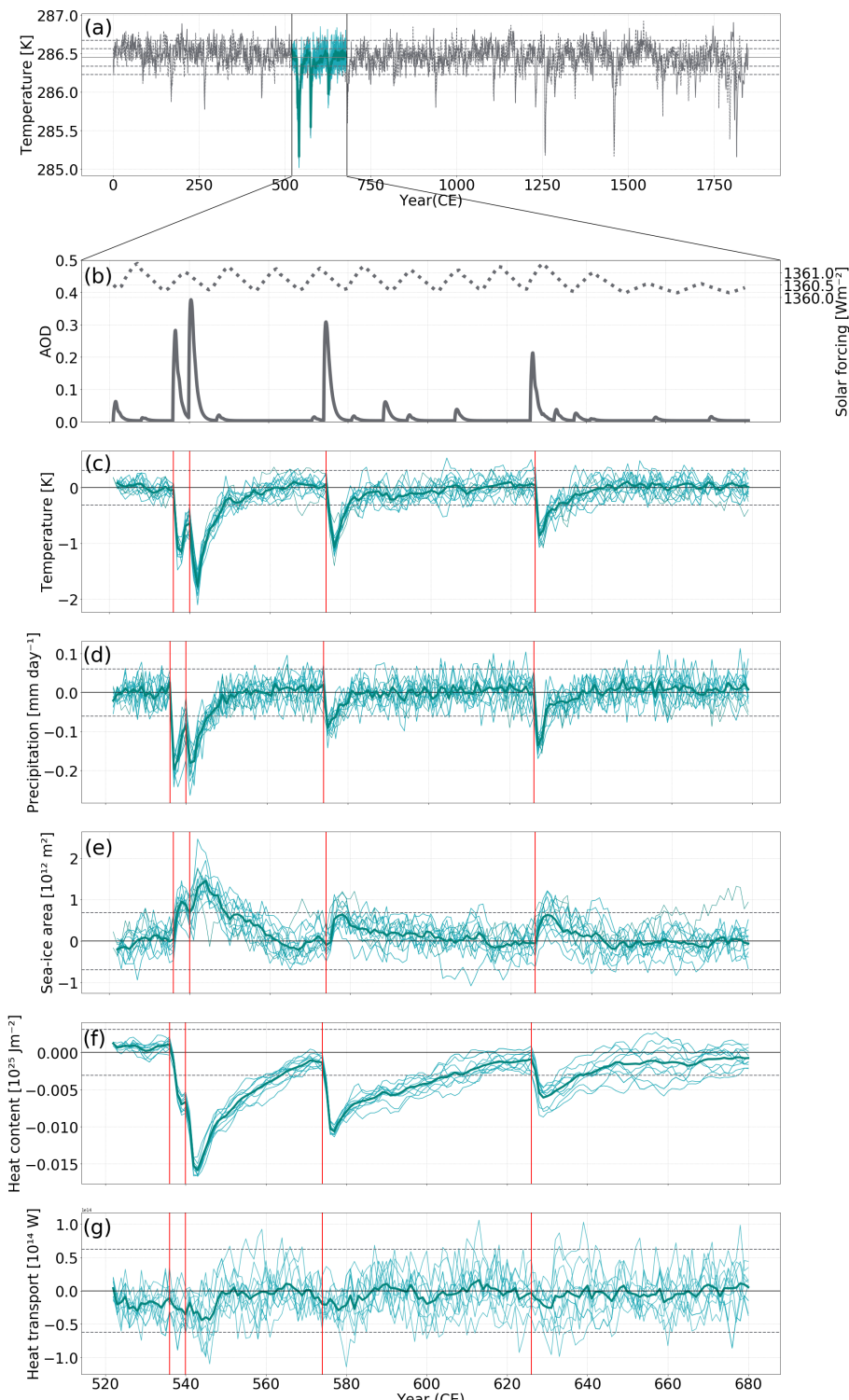


Figure 2. Time series of a) NH 2m air temperature for the two past2k experiments, b) global AOD volcanic forcing and solar forcing. Time series for the MPI-ESM 521-680 CE ensemble runs of c) NH 2m air temperature, d) NH total precipitation, e) Arctic sea-ice area, f) global ocean heat content for the upper 700 m, and g) Atlantic ocean heat transport at 60°N. All variables are given as anomalies wrt 0-1850 CE. The timing of the volcanic eruptions in the study period (520-680 CE) is represented by a red line. Ensemble runs are blue and the ensemble mean is the thick blue line. The grey dashed lines indicate the 2σ of the control run.

Surface climate response

175 To get more insights into the surface climate response we investigate the spatial patterns of the mean short-term (2 years) and long-term (20 years) response following the four large eruptions in Fig 3. The maps show anomalies wrt 0-1850 CE for boreal winter (DJF) and summer (JJA), where the first two winters after the eruption correspond to year 1 and year 2.

180 For boreal winter, the short term response shows the most pronounced near-surface cooling over the Hudson Bay, Labrador Sea, Baffin Bay, and surrounding Western, Southern and Eastern Greenland. The sea level pressure (SLP) anomalies reveal increased pressure over high latitudes poleward of 40-50°N, except for Greenland. At the same time, decreased pressure is visible over the Northern Pacific indicating an eastward shift of the Aleutian low and corresponding wind changes. The 10 m wind shows anomalous westerly flow over the North Atlantic north of 50°N, which means increased westerly winds, and anomalous easterly flow, which means reduced westerly winds, south of ~40 °N. The latitudes north of 40°N show a decrease 185 in precipitation, except for a small area off the west-coast of Norway, whereas south of this latitude it increases. For evaporation there is a land-sea contrast, where south of 40°N there is a decrease over the oceans and an increase over land, and opposite for north of 40°N, with the largest increase in evaporation off the east-coast of Japan. The cloud cover fraction anomaly patterns follow those of precipitation and evaporation closely (not shown).

190 The boreal summer pattern for two years after the eruptions is very similar for 2m air temperature and precipitation. The 2m air temperature is decreased everywhere on the NH, but the cooling is strongest south of ~45°N over the continents (Fig. 3a), which corresponds to the maximum in AOD (Fig. 1). This separation between south and north of 45°N is also visible in the hydrology, where south of 45°N precipitation and evaporation over land increase while they decrease north of it. In summer, the sign of the evaporation anomalies over land and ocean is opposite. The SLP in summer is increased over the polar region and over the continents, except for some areas on the western side in North America and Southern Europe. Over the 195 North Atlantic and the North Pacific, there is a decrease in SLP south of 45°N, with the opposite signal in the SLP anomalies north of this latitude, reflecting an atmospheric circulation separation. The wind anomalies follow the SLP anomaly patterns, with anomalous westerly flow around the decreased low pressure over the Arctic and an anomalous cyclonic pattern around the decreased high pressure systems over the oceans. Wind anomalies above 0.5 m/s only appear over the oceans and coastal regions, not over the continents.

200 In summary, the SLP, precipitation and evaporation maps show a dipole pattern over the NH with a separation at ~40°N in winter and ~45°N in summer, indicating atmospheric circulation changes after two years of the large volcanic eruptions. The wind anomalies show increased surface westerlies north of 60°N, and decreased westerlies south of 50°N over the North Atlantic in NH winter. To get a better insight in the response after each large eruption, the NAO index (see Figure A4 and corresponding text) is given for the entire study period, as well as an epoch analysis for up to 20 years after the four large 205 eruptions. All except the 536 CE eruption show a positive NAO the first winter after the eruption (year 1) followed by a weak positive or a negative second winter. This leads to a weak positive NAO response in the 2-year ensemble mean (Figure 3).

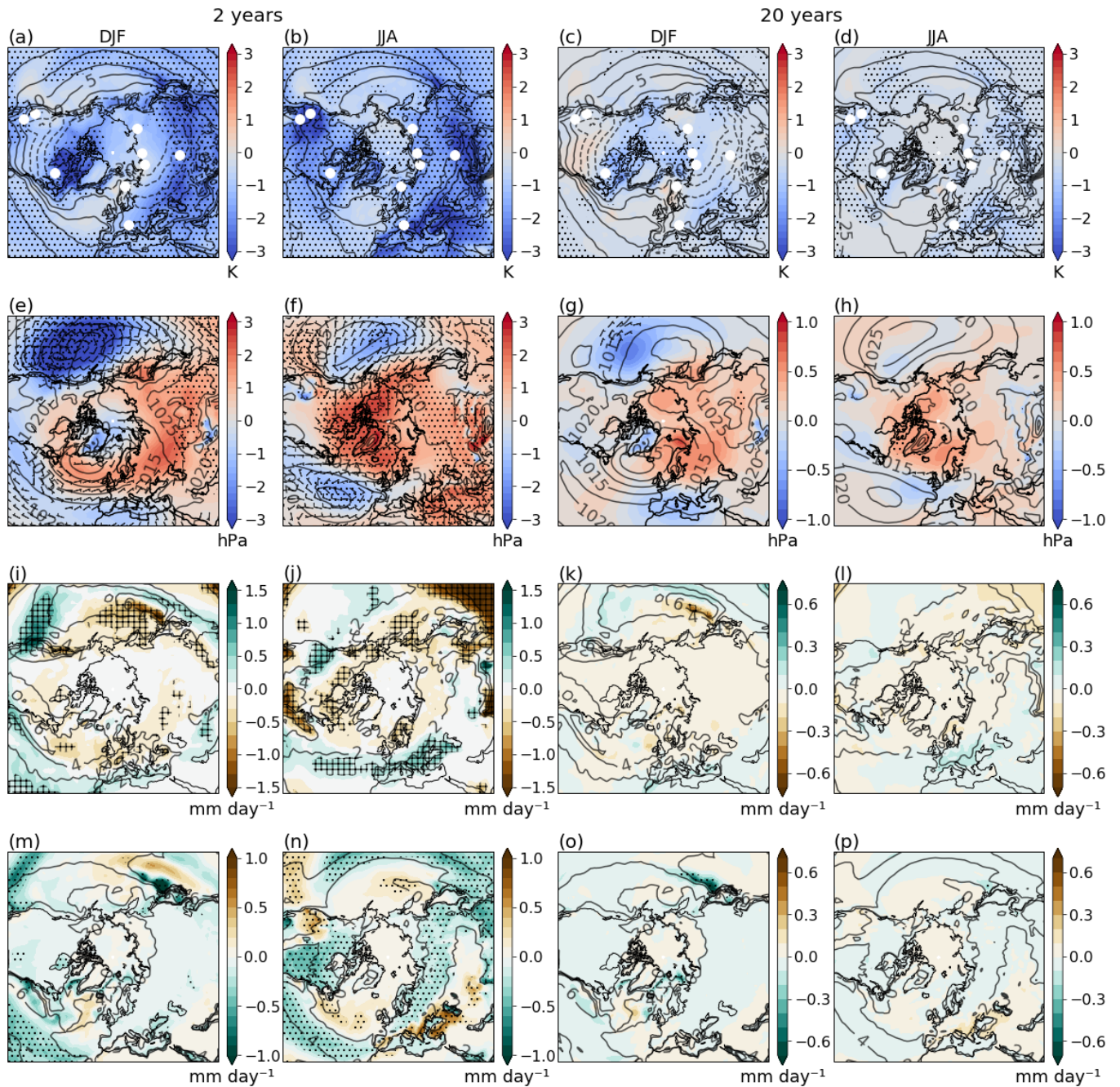


Figure 3. NH maps of boreal winter (DJF) and summer (JJA) 2m air temperature (a-d), sea level pressure and 10 m wind (e-h), precipitation (i-l), and evaporation (m-p) for 2 years and 20 years after the eruptions, poleward of 30°N. The maps represent the ensemble mean of the 2 and 20 year mean after the four major eruptions in the study period. The two years after the eruption are year 1 and year 2 after the eruption for DJF, and the year of the eruption and one year after for JJA, respectively. All variables are given as anomalies wrt 0-1850 CE. The 0-1850 CE climatology is given as contours and the tree-ring locations are represented by white dots in the 2 m air temperature maps. The ensemble standard deviation 1σ (2σ) for 2m air temperature, SLP, evaporation and precipitation are hatched (stippled). Note the different scales for the 2 year and 20 year maps and that wind anomalies are shown only for 105 and 1.0 m/s intervals.

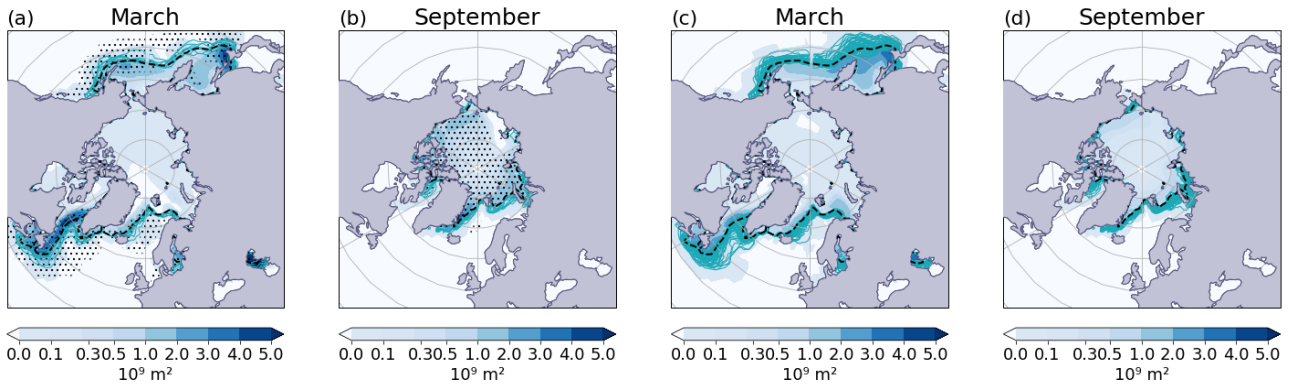


Figure 4. The March and September mean sea-ice area anomaly in contours and the sea-ice extent represented by the teal lines for 2 years after the eruptions (a) and (b) and 20 years after the eruptions (c) and (d). All variables are given as anomalies wrt 0-1850 CE. The black hashed line is the mean sea-ice extent in the control run and the 2σ significant sea-ice area anomalies are stippled.

The sea-ice extent as a response to the eruptions (Figure 4a-b) is given for the maximum and minimum sea ice area months, March and September respectively. For the short term response, the Arctic sea-ice extends southward by at least $\sim 1-2^\circ$ from 210 the long term mean (past2k run 0), with the largest changes south of Greenland to south of Newfoundland and in the Pacific during March and in the Barents Sea and Kara Sea during September.

The long term response is shown in the right panel of Figures 3 and 4. In both winter and summer the patterns are very similar to the 2 year response, only weaker for all variables but the sea-ice extent. For temperature, the main signal that remains is 215 the cooling over the Hudson Bay, the Labrador Sea, east of Greenland towards Svalbard and east of Svalbard in boreal winter. In the same season, the largest SLP anomaly after 20 years is the increased pressure over Scandinavia and Siberia and the decrease over Greenland and the Mediterranean in boreal winter. The sea-ice extent for the long term is extended further south than for the first two years after the eruptions. Especially the Labrador Sea in March and in lesser extend the Barents Sea and Kara Sea in September have an anomalous sea-ice extend, with up to $\sim 5^\circ$ and up to $\sim 3-4^\circ$ from the 0-1850 mean respectively.

220 Overall, the NH maps reveal that there is an atmospheric circulation change with a division at mid-latitudes (around 40°N to 45°N) and a land-sea contrast, where the land shows a larger cooling and the opposite signal for precipitation and evaporation as the ocean, lasting up to 20 years after the four large eruptions, where the long term response is only significant for 2m air temperature.

225 **Ocean - sea-ice response**

Figure 5 shows the time evolution of the barotropic streamfunction (BTS) and the Atlantic meridional overturning circulation (AMOC) from short term (0-2 years), to mid (3-10 years) and long term (11-30 years) response. The BTS corresponds to the horizontal surface flow, and the AMOC corresponds to the vertical mass streamflow in the ocean.

In the first 5 years after the eruptions, there is a decreased transport visible in the BTS from the American east coast all the
230 way to the eastern basin of the North Atlantic of up to 3 Sv (Figure 5a and b). From Fig. 5b and c can be seen that the subpolar
gyre south of Greenland gets more confined to its center 3-10 years after the eruptions, as there is a strengthening of the flow in
the center, whereas the flow at western and eastern sides weakens. At the same time, the transport around 30°- 40°N switches
235 from a weakening to a strengthening flow of more than 3 Sv. After 10 years, the signal in the BTS becomes very small and
after 21-30 years, it is almost all back to around 0 anomaly. The only signal that lingers is the weakened eastern part of the
subpolar gyre, although it does not pass the significance test. The right panels in Fig. 5 reveal a significantly decreased over-
turning circulation that occurs near the surface around 60°N after the first two years and 3-5 years after the eruptions. From
240 3-5 years there is an increase in the streamflow visible at ~2000 m depth, corresponding to a strengthening of the AMOC.
This strengthening peaks at 6-10 years after the eruptions with a significant increase of more than 1 Sv, to decrease again after
10 years. After 20 years the strengthening of the AMOC has disappeared again and the ocean circulation shows hardly any
anomalies. Only the decrease in 2-5 years and the 6-10 year increase in AMOC is significant for this volcanic model ensemble,
which indicates that the long-term AMOC signal is overwhelmed by internal variability.

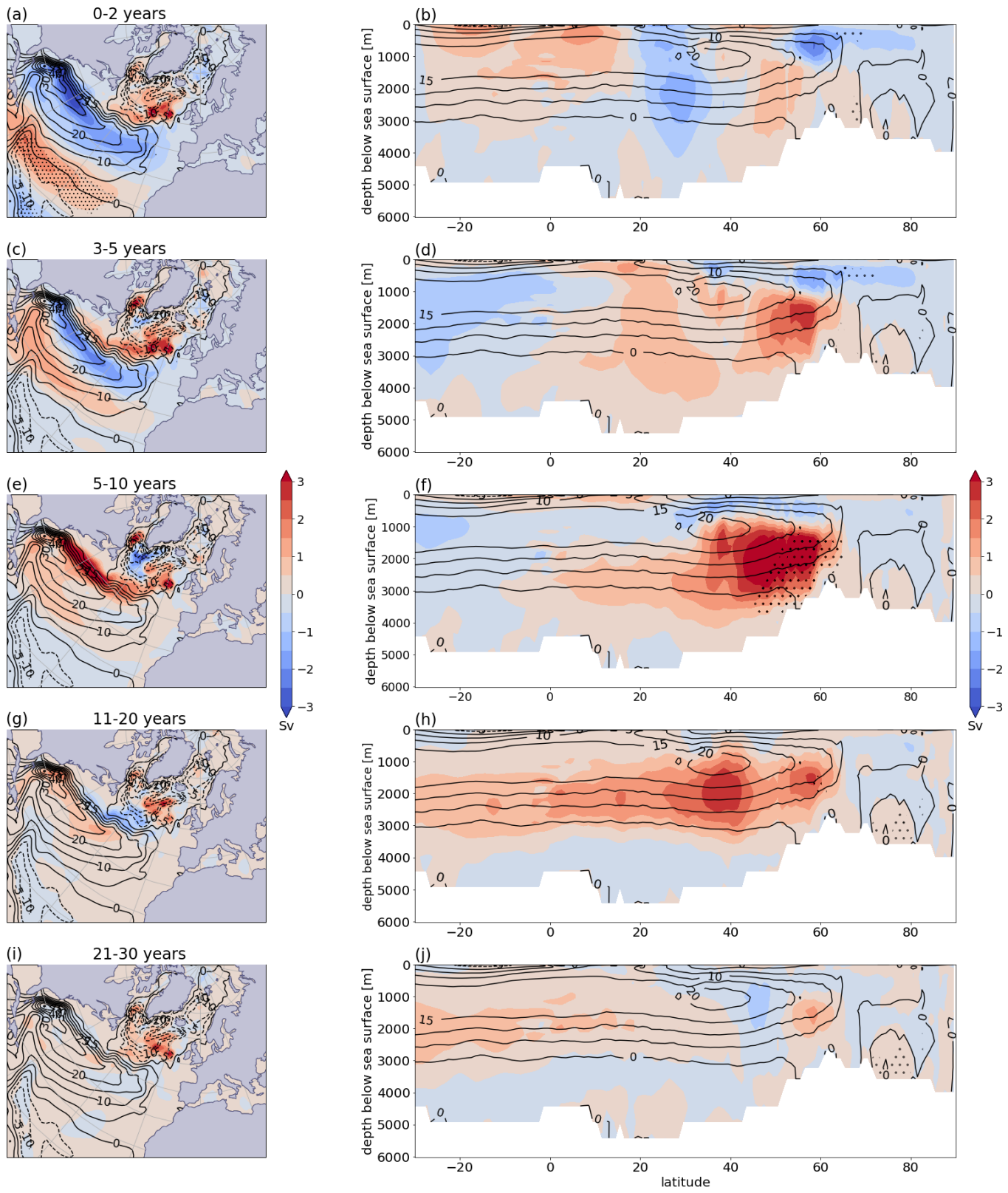


Figure 5.

245 **Figure 5:** (Previous page) Maps of barotropic streamfunction (BTS) and Atlantic meridional overturning circulation (AMOC) ensemble mean anomalies for 2 years (a, b), 3-5 years (c, d), 6-10 years (e, f), 11-20 years (g, h), and 21-30 years (i, j) after the four large eruptions. 0-1850 CE climatology in contours. For the BTS anomaly (left panels), negative absolute values indicate anti-clockwise rotation and positive absolute values indicate clockwise rotation. For AMOC (right panels), negative anomalies correspond to a decrease in stream flow, positive anomalies correspond to an increase in stream flow. Anomalies are with respect to the 0-1850 CE background climatology. 2σ significant areas are stippled.

Tree-ring - model comparison

250 We compare the 2m air temperatures from the model simulations to ensemble reconstructions from tree-ring data from Büntgen et al. (2021). For the model - tree-ring comparison, the model temperature anomalies were taken for NH land only, JJA and 40-75°N, to correspond as closely to the tree-ring data as possible.

255 In general, there is a good agreement between the 520-680 CE simulations and the tree-ring data for the NH. The reconstructed NH temperatures from the ensemble mean fall within the spread of the model simulations. The peak cooling for the model simulations show a larger cooling than for the tree-ring data, with a maximum cooling of more than 2.0 K for the model and 1.2 K for the tree-ring ensemble mean after the 536 CE eruption.

The temperature recovery is not the same for the tree-ring ensemble and the model ensemble. After the 536/540 CE double eruption, the modeled temperature recovers faster than the reconstructed temperature. For the other two large volcanic eruptions, the opposite happens, where the tree-ring reconstructed temperatures recover faster than the modeled temperatures.

260 Another discrepancy that catches attention is the smaller NH extratropical eruptions. In the reconstructed temperature these eruptions give a small but distinct cooling peak, but in the model simulated temperatures they are not visible as such. We will discuss discrepancies in the discussion section.

265 Lastly, the timing of the peak cooling after the four large volcanic eruptions agrees very well. Except the timing of the 626 CE eruption is shifted by one year, which is due to the fact that unknown eruptions are set to January in the model forcing. However, documentary evidence suggests the eruption took place in autumn as described by Sigl et al. (2015). Thus, the trees responded the summer after the eruption, whereas the temperatures in the model simulations responded in the year of the eruption.

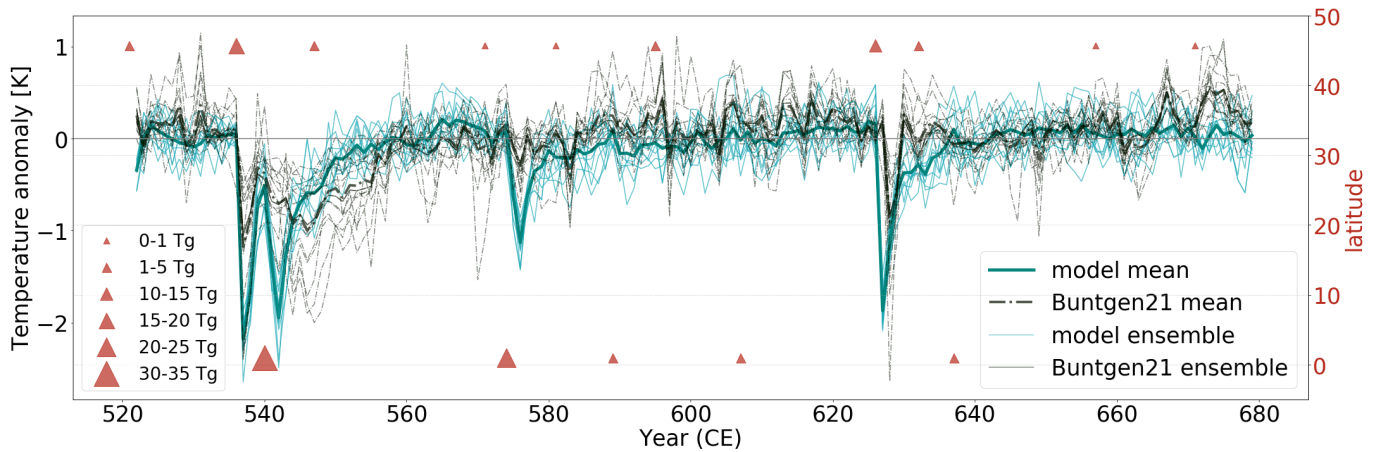


Figure 6. Model–tree-ring comparison for the NH. The model 2m air temperature anomalies are taken for land only, JJA and 40 to 75 °N. The tree-ring data is from Büntgen et al. (2021). Mean anomalies are calculated for the 0–1850 CE reference period. The red triangles represent the volcanic eruptions from the model forcing according to their latitude (tropical or NH extratropical), and the size of the triangle corresponds to the estimated range of sulphur [Tg S] injected into the stratosphere (Toohey and Sigl, 2017).

4 Discussion

In this section, we discuss the results in a chronological order focusing on the most outstanding features.

270 Volcanic response

There is a strong cooling visible around the mid-latitudes in Fig. 3a, which corresponds to the peak accumulated AOD in the volcanic forcing (Fig. 1). The volcanic forcing used for this study is based on eVolv2k (Toohey and Sigl, 2017, see section 2.1.4), which gives the peak AOD at a latitude of 45°N (Fig. A5). The accumulated AOD is calculated for 15 years, to compare to Toohey et al. (2016a). The model reconstruction for the 536/540 eruption double event by (Toohey et al., 2016a, see also

275 Table 1) led to the maximum accumulated AOD in the Arctic at around 75°N. The simulated maximum cooling in mid latitudes at around 30–40°N in the Mediterranean, the Himalayas and the Western United States that we see in this study are the same areas as Toohey et al 2016a simulated. However, the cooling in our study is stronger, which could be due to the latitudinal difference of the peak volcanic forcing between the two studies. The fact that the difference in latitude for the peak AOD gives the same cooling patterns points to this not being from the direct effects of the volcanic aerosols.

280 Atmospheric circulation changes

In boreal winter, there is a see-saw pattern visible in the 2 year SLP response with decreased pressure over Greenland and an increase in pressure over Northern Europe, corresponding to the seesaw winter temperature pattern observed between Greenland and Scandinavia, as described by Van Loon and Rogers (1978). Next, the hemispheric changes in boreal winter reflect

285 a positive Arctic Oscillation pattern, as described by Thompson and Wallace (1998), and typically observed after volcanic eruptions (Robock and Mao, 1992; Stenchikov et al., 2006).

After the volcanic eruptions, the climatological high pressure center over the Atlantic in the mid-latitudes gets more confined, which leads to the surface climate patterns with a separation at $\sim 45^{\circ}\text{N}$. From Fig. 3, the 2m air temperature, precipitation and SLP anomalies do not show a clear positive NAO phase for the first two years after the four large eruptions, but from Figure A4 can be seen that the ensemble simulates a positive NAO response in the first year after three of the four large eruptions. There is
290 a very small, non-significant warming over western Scandinavia and northwest Siberia in the DJF 2m air temperature anomaly, hinting towards a regional surface winter warming. Bittner et al. (2016a) analyzed a 100 member ensemble to study the polar vortex and NAO response after volcanic eruptions in the tropics, and they concluded that for large eruptions (Krakatoa/Pinatubo size) at least 15 ensemble members are necessary to get a significant response on the polar vortex. A surface winter warming pattern and a positive NAO has been observed after large tropical eruptions in the past (Robock and Mao, 1992; Robock, 2000).
295 However, not all IPCC models show this signal (Stenchikov et al., 2002; Driscoll et al., 2012). The cause for this is still highly debated. A few of the debated points are about discussing model deficiencies (low top versus high top models, Charlton-Perez et al., 2013), volcanic aerosol forcing details (Toohey et al., 2014), strength of the volcanic eruption and forcing (Bittner et al., 2016b), tropical versus high latitude eruption impact (Schneider et al., 2009), the role of the ENSO state during the eruption (Coupe and Robock, 2021), up to if the observed signal is due to volcanic eruptions at all (Polvani et al., 2019). Here, we use a
300 mean of 12 ensemble members, 4 eruptions, and a mix of tropical and extratropical eruptions, which could dampen the signal.

Hydrological cycle changes

The increase in precipitation over the Mediterranean in boreal summer 2 years after the eruptions in the model simulations in this study are related to the shifting of the inter tropical convergence zone (ITCZ) into the Southern Hemisphere (SH) after the eruptions (not shown here), as well as a weakening of the high and low SLP over the North Atlantic (Figure 3b). After a large
305 volcanic eruption, the ITCZ shifts away from the hemisphere that experiences the strongest cooling (Schneider et al., 2009), in this case the NH. The southward shift in the ITCZ leads to a weakening of the northern branch of the Hadley cell (Wegmann et al., 2014), which leads to a lower high pressure over southern Europe. This in turn leads to a wetter Mediterranean region, especially in summer (3b-c). Another pattern that becomes evident in the boreal summer months is the land-sea contrast. Over the continents there is a high pressure anomaly, whereas over the oceans there is a low pressure anomaly. This could be due to
310 the radiative effect, where the land responds faster to the cooling effect of the volcanic aerosols.

In addition, the evaporation is increased where the precipitation is also increased, and vice versa. This indicates that the evaporation is more driven by soil moisture availability than by temperature changes. In a colder atmosphere, the air cannot hold as much moisture and becomes saturated sooner, limiting the evaporation (Bala et al., 2008). If the evaporation is driven by the change in temperature one would expect the evaporation to decrease with decreasing 2m air temperature. In this case, there is an increase in precipitation over areas with the strongest cooling, like the Mediterranean, leading to more water being
315 available for evaporation. North of 45°N over the continents, the evaporation anomaly decreases, which corresponds to the

decrease in precipitation.

The simulated wettening over the Mediterranean and the drying over Northern Europe in boreal summer is consistent with
320 other studies. Iles et al. (2013) used HadCM3 and concluded the mean response to 18 eruptions during 1442-1992 to be a wet-
ttening over the Mediterranean and a drying of Northern Europe for up to 4 years after the eruptions during the summer season.
Interestingly, our results on hydroclimate and SLP are in accordance with Liu et al. (2020), who used the Community Earth
325 System Model (CESM) to simulate the volcanic effect of the Samalas 1258 CE eruption on the surface climate. In their study,
they concluded that the dipole between the drying over Northern Europe and the wettening of the Mediterranean is a result of
the weakening of the pressure systems over the North Atlantic and the resulting wind anomalies, as we found in this study for
330 the 521-680 CE ensemble as well. Fischer et al. (2007) found a wettening over the Mediterranean the year of eruption, which
disappeared the 1 year after, and Rao et al. (2017) found a wettening over the Mediterranean lasting up to 5 years, where it
was significant in the western part. The low significance for the precipitation response could be due to the large noise, which
drowns out the volcanic signal (Fischer et al., 2007).

330

Hardly any studies have studied the long term response for hydrology after volcanic eruptions. Stevenson et al. (2018) argue
335 that volcanic influences on the multidecadal hydroclimate variability is connected to the Atlantic multidecadal oscillation
(AMO) teleconnections, which relates to our results of the SLP anomalies and the corresponding hydroclimate anomaly patterns.
However, their focus is on tropical regions and not on the NH mid- to high latitudes. In our simulations, the precipitation
and evaporation long term response show the same pattern as for two years after the eruptions, but this is not significant.

The SLP anomaly in the long term response over the Barents Sea and Kara Sea corresponds to the sea-ice extent in September.
The increase in sea-ice leads to lower air temperature above this area, which causes the air to descend, increasing the SLP.
The extended sea-ice in Labrador Sea is important for ocean and sea-ice interactions, which impacts the ocean circulation in
340 the North Atlantic (Zhong et al., 2011; Moreno-Chamarro, 2016).

340 **Ocean - sea-ice response**

Zhong et al. (2011), and Miller et al. (2012) argued that the ocean - sea-ice feedback could play a major role in sustaining a
345 century long cooling after a cluster of four volcanic eruptions in the mid 13th century. In contrast to these studies, our simulated
cooling is shorter and lasts for several decades. After the 536/540 CE double event, the sea-ice cover in the ensemble mean
takes longer to recover and does not reach the climatological mean value until the year 560 CE. This means that the sea-ice is in
an anomalous state for more than 20 years after the 536 CE eruption. Following the 574 eruption, the sea-ice area is anomalous
350 for 30 years, and after the 626 eruption the sea-ice area is anomalous for 15 years.

The ocean - sea-ice feedback can help to maintain the long-lasting cooling in the NH. A complex interaction between sea-ice
expansion, changes in horizontal circulation (BTS) and overturning circulation leads to the reduction in heat transport, which
355 then further enhances sea-ice expansion (Zhong et al., 2011). In our simulations, the sea-ice expansion is most pronounced

in the Labrador Sea, which results in a confinement of the subpolar gyre to its center south of Greenland, where it shows a strengthening of ~ 3 Sv 2-10 years after the eruptions (5b and c). At the same time, the cyclonic circulation weakens by more than 3 Sv in the eastern basin, which goes along with a reduction of the gyre related heat transports, as described by Jungclaus et al. (2014). In addition, there is a reduction in the Gulf Stream of more than 3 Sv in the first 5 years, followed by 355 a strengthening of the same magnitude in years 6-10. This is consistent with Zanchettin et al. (2012), although they found the strengthening to occur later, 11-15 years after the eruption.

In the first 5 years after the eruption, we diagnose a decreased transport in the BTS from the American east coast to the 360 eastern Basin of the North Atlantic. This decrease reflects a weakening of the anticyclonic subtropical gyre (STG) and it occurs most pronounced in the Gulf Stream region. Positive BTS anomalies at the eastern side of the cyclonic subpolar gyre (SPG) indicate a weakening of the gyre circulation there, whereas negative anomalies south of Greenland point to a strengthening 365 of the gyre center. The weaker gyre circulation in the eastern basin can be associated with less gyre-driven heat transports at mid-latitudes (Moreno-Chamarro et al., 2017). After 5 years, the STG anomalies reverse, probably by changes in the wind forcing, whereas the SPG anomalies in the gyre center and its eastern side are retained. We note, however, that these changes do not pass the significance criterion and we assume that therefore also the changes in the heat transport at 60°N (which should 370 be largely gyre-driven) are consistent with the increased sea-ice extend, but not statistically significant.

As for the overturning circulation, the expanded sea-ice in the Labrador Sea leads to a deep water formation outside the 375 normal deep water formation areas further south. The sea-ice formation process includes brine rejection, which leads to saltier, and thus more dense surface waters (Zhong et al., 2011), initiating overturning and thus leading to the deep water formation and an increased AMOC from 5 up to 20 years after the eruptions in this study. The increased AMOC then in turn corresponds to the positive anomaly in the subtropics to mid-latitudes of the BTS. Halloran et al. (2020), analyzing oxygen isotope variability recorded from Iceland and the PMIP3 last millennium ensemble, concluded that the same feedback cycle took place in 380 the pre-industrial millennium. In addition, they demonstrate that a third of the multidecadal Arctic sea-ice variability can be explained by natural external forcing.

375 Zanchettin et al. (2012) simulated the ocean-atmosphere response to large volcanic eruptions, and concluded that the sea-ice extent and corresponding deep ocean convection in the North Atlantic was dependent on the initial state of the ensemble member. This led to different model ensembles having different spatial patterns when it comes to deep convection in the North Atlantic. The study from Zhong et al. (2011) about the onset of the LIA also concluded the response to be depended on the initial state of the North Atlantic, as only 2 out of 4 simulations (one warm and one normal NA state) lead to a cooling long 380 enough to resemble the LIA. It was part of our experiment design to start the ensemble simulation from an ocean state representing 520 CE conditions and to create the model's ensemble spread by perturbing the atmosphere. While this was done to include a proper representation of the forcing history in the previous decades, it does not allow us to investigate the effects of different ocean initial conditions (for this, an ensemble of past2k simulation would have been needed). It is therefore possible that the ensemble spread is underestimated. Another choice would have been to start the model integration from different states 385 of the AMOC Pohlmann et al. (2004). An inspection of the AMOC time series, however, (Fig. A4 d) reveals that the AMOC

variations do diverge quite rapidly after the start of the experiment and show a similar range at the time of the first major eruption compared to the end of the experiment. The only quantity where we see an increase of ensemble spread throughout the experiment is the global ocean heat content.

390 Another reason for the different responses between the studies described above, besides the different models used and the difference in initial conditions, could be the difference in volcanic forcing. The climate simulations are sensitive to both the climate model and the volcanic forcing, so using different ones will give a different climate response. This will be the more likely reason for the lack of consensus, as 10 ensemble members were run, which showed a range of variability in the ocean variables that are in the same range as the 0-1850 CE variability, and the response to the volcanic eruptions clearly stood out
395 against this, see for example Fig. 2. Other studies (Zanchettin et al., 2012; Zhong et al., 2011; Lehner et al., 2013) used a range of different background conditions in the beginning of their model simulations and found similar results as we did, despite the background conditions set-up. Zanchettin et al. (2016) showed that there are large uncertainties between different volcanic forcing sets that have been used for different modeling studies. Previously used forcings, like for example Gao et al. (2008); Crowley and Unterman (2013), have a range of very different AOD evolutions over time after a eruption. Some forcings give
400 a very high peak but a short lifetime, while others have a lower and later peak AOD and a longer lifetime. In addition, the eruption season is also important for the surface response. Different eruption seasons give different surface responses (Toohey et al., 2011). These different forcings will give different responses of the surface climate in an ESM simulation. The volcanic forcing used in this study is the same as for PMIP4, which makes it easier to compare different model runs for this period. Further research into the role of different forcing sets and different responses between the models is needed to fully understand
405 this lack of consensus in the response timing between the studies. This could be a task within for example the Volcanic Forcing Model Intercomparison Project (VolMIP, Zanchettin et al., 2016).

Model - tree-ring comparison

The model - tree-ring comparison with the tree-ring ensemble reconstruction (Fig. 6) shows a very good agreement in especially the timing of the 2 m air temperature anomalies and the recovery time of ~20 year after the peak cooling for the NH extratropics
410 land only JJA. The mismatches that are still present in this NH comparison, like the strength of the peak cooling, as well as the lag after the 536/540 CE eruptions, include potential deficiencies and uncertainties regarding both methods. For example, on the tree ring side TRW was used, which is known to give a lagged and smoothed response (Zhang et al., 2015; Esper et al., 2015; Lücke et al., 2019; Zhu et al., 2020). Reconstructions are becoming more uncertain further back in time due to the sparseness of available proxy records, especially before 1200 CE (Masson-Delmotte, 2013; Esper et al., 2018; Neukom et al.,
415 2019). Comparing the model results with temperature reconstructions for the entire NH annual mean (Neukom et al., 2019) reveals a less good agreement (see Appendix A, Figure A3). Concerning the simulations, Timmreck et al. (2021) showed that beyond model deficiencies, choices regarding both volcanic forcing strength and spatial structure can similarly affect reconstruction–simulation comparisons. Hence, a potential reason for the offset could be that the forcing of the moderate eruption in 547 CE is underestimated. Other smaller NH extratropical eruptions also have a weaker temperature signal in the

420 modeled temperature response, which could point to an underpresentation of the volcanic forcing of small to medium size eruptions.

The EVA forcing generator that was used to get the AOD input for the model (see methods) was based on tropical eruptions (Toohey et al., 2016b) and might therefore not simulate the processes and related timescales for relatively small eruptions in the extratropics. The fact that the eruption dates are always put to January if unknown also could influence the simulated response
425 (Toohey et al., 2011; Stevenson et al., 2017; Toohey et al., 2019).

The concept of a LALIA was raised by Büntgen et al. (2016), based on tree-ring data from the Alps and Altai. Comparing these specific sites as well, the model and tree-ring reconstruction do not agree as for the NH tree ring ensemble reconstruction, and especially the Altai reconstruction shows a longer cooling after the 536/540 CE eruptions (Figure A2b and c). Previous
430 proxy-based studies (Larsen et al., 2008; Esper et al., 2012b; Luterbacher et al., 2016; Helama et al., 2017; Neukom et al., 2019) found a cooling up to 570 CE for Scandinavia, Europe, and the NH, based on tree-ring, ice-core, lake sediment, and documentary records (Figures A2a and d, and A3).

From the perspective of our model results, the persistence of the cooling was not as long lasting as the tree-ring sites from the Alps and Altai suggested. Perhaps the century-long lasting cooling may be only apparent in the Alps and Altai tree-ring
435 records, as a regional feature occurring at high altitude of the mid-latitudes. Another possibility is, that our model resolution is too coarse to fully capture the topography of the mountains in the Alps and the Altai or that the evolution of glaciers, which is not accounted for in the model, could explain why the model simulations deviate in these areas. Glacier fluctuations from the last 2000 years show glaciers in the Alps advancing during this period, lasting for \sim a century (Solomina et al., 2016). Ice core records from Greenland (Sigl et al., 2015) agree well with the tree-ring data from Alps (Büntgen et al., 2016). The LIA also
440 had regional variability and was also punctuated with warmer periods (Mann, 2002). The regional variability of the LALIA is a topic to be further investigated in future studies.

Moreover, the study from Büntgen et al. (2021) shows that it is important to also use an ensemble when it comes to tree-ring reconstructions, as the different statistical methods used to analyze the data give different reconstructions. In addition, the reality can be viewed as one iteration of what could have happened under different initial conditions, ocean states and internal
445 variability. Taking into account the entire range of ensemble members is therefore important.

Our model ensemble set up with the PMIP4 volcanic forcing reveals up to 25 years of surface cooling over land of the NH extratropics during summer and it also shows the distinct atmospheric circulation response pattern for precipitation and evaporation at \sim 40°N, separating the Alps and Altai from the other tree-ring locations. The change in hydro-climate corresponds to the soil moisture availability for the trees and thus could have impacted tree ring growth (Bassett, 1964; Müller et al.,
450 2016). Future studies are needed to further investigate the temperature, atmospheric circulation, and hydro-climate response in a multi-model context and investigate regional differences in the tree-ring records, as well as the response to tropical and extratropical eruptions.

5 Summary and Conclusions

455 In this study, we analyzed new climate model ensemble simulations from 520-680 CE with the MPI-ESM model and PMIP4 volcanic forcing. The aim was to get insights if a series of volcanic eruptions starting with the 536/540 CE double event would lead to a long lasting cooling in the mid 6th to 7th century in the Northern Hemisphere (NH).

460 In summary, we find that a series of four large and several small to medium size volcanic eruptions lead to a significant regional peak cooling up to 3 K in the NH. In addition, atmospheric circulation changes with a hemispheric dipole structure separated at around 40-45°N and a land-sea contrast pattern occurs. Analyzing underlying mechanisms in the North Atlantic reveal that complex interaction between sea-ice expansion, changes in the barotropic streamfunction and the Atlantic meridional overturning circulation lead to a reduction in the ocean heat transport, which then further enhances sea ice expansion impacting NH surface climate up to 20 years.

465 The modelled volcanic induced multi-decadal large scale NH cooling is consistent with tree ring ensemble reconstructions for this period. This shows that the ocean - sea-ice sustained ~20 year cooling as occurring in our simulations is a plausible mechanism. The simulated dipole in the atmospheric circulation during summer could hold clues for the difference in the tree-ring reconstructions for the Alps and Altai sites, which show a century long cooling. Future model studies comparing different models and volcanic forcing with each other will be useful for verifying our results.

470 The summer cooling can have a serious effect on vegetation and society, as a few degrees cooling in summer can lead to crop failure and famine in areas that are close to the temperature limit for growing crops. In a follow-up study, we will investigate if and how large volcanic eruptions in the mid-6th century may have impacted climate and society in Scandinavia by using the model simulations from this study and combining it with a local model as well as climate proxy and archaeological records.

475 *Code and data availability.* Primary data and scripts used in the analysis and other supplementary information that may be useful in reproducing the author's work are archived and can be obtained by request. Model results will be available under cera-www.dkrz.de. The PMIP4 past2k simulations contribute to CMIP6 and can be retrieved via the Earth System Grid Federation network (e.g., <https://esgf-data.dkrz.de/search/cmip6-dkrz/>). Tree-ring proxy data can be obtained from NOAA/World Data Service for Paleoclimatology archive <https://www.ncdc.noaa.gov/access/paleo-search/study/33215>.

480 *Author contributions.* KK, CT and EvD conceived the original idea. EvD, CT, JJ and SL planned the model simulations. SL and JJ designed the model and the computational framework. EvD carried out the model runs, processed the data, performed the analysis, and designed the figures. KK, CT, JJ contributed to the interpretation of the results. KK supervised the project. All authors discussed the results and helped writing the manuscript.

Competing interests. The authors declare they have no competing interest.

Acknowledgements. This work is funded by the NFR/UiO Toppforsk project "VIKINGS" with the grant number 275191. Computations, analysis and model data storage were mainly performed on the computer of the Deutsches Klima Rechenzentrum (DKRZ), and partly on
485 Sigma2 the National Infrastructure for High Performance Computing and Data Storage in Norway. CT acknowledges support to this research by the Deutsche Forschungsgemeinschaft Research Unit VolImpact (FOR2820,398006378) within the project VolClim (TI 344/2-1). Thanks to Ulf Büntgen, Matthew Toohey, and Michael Sigl for discussions on the results, and to Davide Zanchettin for his help with the significance calculations. Thanks to MPI for Meteorology Hamburg to make a guest exchange possible, which led to the idea for new model experiments of this paper.

Anchukaitis, K. J., Breitenmoser, P., Briffa, K. R., Buchwal, A., Büntgen, U., Cook, E. R., D'arrigo, R. D., Esper, J., Evans, M. N., Frank, D., et al.: Tree rings and volcanic cooling, *Nature Geoscience*, 5, 836–837, 2012.

Baillie, M. G.: Proposed re-dating of the European ice core chronology by seven years prior to the 7th century AD, *Geophysical Research Letters*, 35, 2008.

495 Bala, G., Duffy, P., and Taylor, K.: Impact of geoengineering schemes on the global hydrological cycle, *Proceedings of the National Academy of Sciences*, 105, 7664–7669, 2008.

Bassett, J. R.: Tree growth as affected by soil moisture availability, *Soil Science Society of America Journal*, 28, 436–438, 1964.

Bittner, M., Schmidt, H., Timmreck, C., and Sienz, F.: Using a large ensemble of simulations to assess the Northern Hemisphere stratospheric dynamical response to tropical volcanic eruptions and its uncertainty, *Geophysical Research Letters*, 43, 9324–9332, 2016a.

500 Bittner, M., Timmreck, C., Schmidt, H., Toohey, M., and Krüger, K.: The impact of wave-mean flow interaction on the Northern Hemisphere polar vortex after tropical volcanic eruptions, *Journal of Geophysical Research: Atmospheres*, 121, 5281–5297, 2016b.

Briffa, K. R., Jones, P. D., Schweingruber, F. H., and Osborn, T. J.: Influence of volcanic eruptions on Northern Hemisphere summer temperature over the past 600 years, *Nature*, 393, 450–455, 1998.

Büntgen, U., Tegel, W., Nicolussi, K., McCormick, M., Frank, D., Trouet, V., Kaplan, J. O., Herzig, F., Heussner, K.-U., Wanner, H., et al.: 505 2500 years of European climate variability and human susceptibility, *Science*, 331, 578–582, 2011.

Büntgen, U., Myglan, V. S., Ljungqvist, F. C., McCormick, M., Di Cosmo, N., Sigl, M., Jungclaus, J., Wagner, S., Krusic, P. J., Esper, J., et al.: Cooling and societal change during the Late Antique Little Ice Age from 536 to around 660 AD, *Nature Geoscience*, 9, 231, 2016.

Büntgen, U., Arseneault, D., Boucher, É., Churakova, O. V., Gennaretti, F., Crivellaro, A., Hughes, M. K., Kirdyanov, A. V., Klippel, L., Krusic, P. J., et al.: Prominent role of volcanism in Common Era climate variability and human history, *Dendrochronologia*, 64, 125–157, 510 2020.

Büntgen, U., Allen, K., Anchukaitis, K. J., Arseneault, D., Boucher, É., Bräuning, A., Chatterjee, S., Cherubini, P., Churakova, O. V., Corona, C., et al.: The influence of decision-making in tree ring-based climate reconstructions, *Nature communications*, 12, 1–10, 2021.

Charlton-Perez, A. J., Baldwin, M. P., Birner, T., Black, R. X., Butler, A. H., Calvo, N., Davis, N. A., Gerber, E. P., Gillett, N., Hardiman, S., et al.: On the lack of stratospheric dynamical variability in low-top versions of the CMIP5 models, *Journal of Geophysical Research: Atmospheres*, 515 118, 2494–2505, 2013.

Consortium, P. et al.: A global multiproxy database for temperature reconstructions of the Common Era, *Scientific data*, 4, 2017.

Coupe, J. and Robock, A.: The Influence of Stratospheric Soot and Sulfate Aerosols on the Northern Hemisphere Wintertime Atmospheric Circulation, *Journal of Geophysical Research: Atmospheres*, p. e2020JD034513, 2021.

Crowley, T. J. and Unterman, M. B.: Technical details concerning development of a 1200 yr proxy index for global volcanism, *Earth System Science Data*, 5, 187–197, 2013.

520 Driscoll, S., Bozzo, A., Gray, L. J., Robock, A., and Stenchikov, G.: Coupled Model Intercomparison Project 5 (CMIP5) simulations of climate following volcanic eruptions, *Journal of Geophysical Research: Atmospheres*, 117, 2012.

Esper, J., Büntgen, U., Timonen, M., and Frank, D. C.: Variability and extremes of northern Scandinavian summer temperatures over the past two millennia, *Global and Planetary Change*, 88, 1–9, 2012a.

525 Esper, J., Frank, D. C., Timonen, M., Zorita, E., Wilson, R. J., Luterbacher, J., Holzkämper, S., Fischer, N., Wagner, S., Nievergelt, D., et al.: Orbital forcing of tree-ring data, *Nature Climate Change*, 2, 862–866, 2012b.

Esper, J., Schneider, L., Smerdon, J. E., Schöne, B. R., and Büntgen, U.: Signals and memory in tree-ring width and density data, *Dendrochronologia*, 35, 62–70, 2015.

Esper, J., George, S. S., Anchukaitis, K., D'Arrigo, R., Ljungqvist, F. C., Luterbacher, J., Schneider, L., Stoffel, M., Wilson, R., and Büntgen, U.: Large-scale, millennial-length temperature reconstructions from tree-rings, *Dendrochronologia*, 50, 81–90, 2018.

Eyring, V., Bony, S., Meehl, G. A., Senior, C. A., Stevens, B., Stouffer, R. J., and Taylor, K. E.: Overview of the Coupled Model Intercomparison Project Phase 6 (CMIP6) experimental design and organization, *Geoscientific Model Development*, 9, 1937–1958, 2016.

Fischer, E. M., Luterbacher, J., Zorita, E., Tett, S., Casty, C., and Wanner, H.: European climate response to tropical volcanic eruptions over the last half millennium, *Geophysical research letters*, 34, 2007.

Gao, C., Oman, L., Robock, A., and Stenchikov, G. L.: Atmospheric volcanic loading derived from bipolar ice cores: Accounting for the spatial distribution of volcanic deposition, *Journal of Geophysical Research: Atmospheres*, 112, 2007.

Gao, C., Robock, A., and Ammann, C.: Volcanic forcing of climate over the past 1500 years: An improved ice core-based index for climate models, *Journal of Geophysical Research: Atmospheres*, 113, 2008.

Gleckler, P., AchutaRao, K., Gregory, J., Santer, B., Taylor, K., and Wigley, T.: Krakatoa lives: The effect of volcanic eruptions on ocean heat content and thermal expansion, *Geophysical Research Letters*, 33, 2006.

Halloran, P. R., Hall, I. R., Menary, M., Reynolds, D. J., Scourse, J. D., Screen, J. A., Bozzo, A., Dunstone, N., Phipps, S., Schurer, A. P., et al.: Natural drivers of multidecadal Arctic sea ice variability over the last millennium, *Scientific reports*, 10, 1–9, 2020.

Hegerl, G. C., Crowley, T. J., Hyde, W. T., and Frame, D. J.: Climate sensitivity constrained by temperature reconstructions over the past seven centuries, *Nature*, 440, 1029–1032, 2006.

Helama, S., Jones, P. D., and Briffa, K. R.: Limited late antique cooling, *Nature Geoscience*, 10, 242–243, 2017.

Hurrell, J. W.: Decadal trends in the North Atlantic Oscillation: regional temperatures and precipitation, *Science*, 269, 676–679, 1995.

Hurt, G. C., Chini, L., Sahajpal, R., Frolking, S., Bodirsky, B. L., Calvin, K., Doelman, J. C., Fisk, J., Fujimori, S., Goldewijk, K. K., et al.: Harmonization of global land-use change and management for the period 850–2100 (LUH2) for CMIP6, *Geoscientific Model Development Discussions*, pp. 1–65, 2020.

Iles, C. E., Hegerl, G. C., Schurer, A. P., and Zhang, X.: The effect of volcanic eruptions on global precipitation, *Journal of Geophysical Research: Atmospheres*, 118, 8770–8786, 2013.

Jungclaus, J., Fischer, N., Haak, H., Lohmann, K., Marotzke, J., Matei, D., Mikolajewicz, U., Notz, D., and Von Storch, J.: Characteristics of the ocean simulations in the Max Planck Institute Ocean Model (MPIOM) the ocean component of the MPI-Earth system model, *Journal of Advances in Modeling Earth Systems*, 5, 422–446, 2013.

Jungclaus, J., Bard, E., Baroni, M., Braconnot, P., Cao, J., Chini, L., Egorova, T., Evans, M., González-Rouco, J. F., Goosse, H., et al.: The PMIP4 contribution to CMIP6–Part 3: The last millennium, scientific objective, and experimental design for the PMIP4 past1000 simulations, 2017.

Jungclaus, J. H., Lohmann, K., and Zanchettin, D.: Enhanced 20th century heat transfer to the Arctic simulated in context of climate variations over last millennium, *Climate of the Past*, 10, 2201–2213, 2014.

Kageyama, M., Albani, S., Braconnot, P., Harrison, S. P., Hopcroft, P. O., Ivanovic, R. F., Lambert, F., Marti, O., Peltier, W. R., Peterschmitt, J. Y., et al.: The PMIP4 contribution to CMIP6-Part 4: Scientific objectives and experimental design of the PMIP4-CMIP6 Last Glacial Maximum experiments and PMIP4 sensitivity experiments, *Geoscientific Model Development*, 10, 4035–4055, 2017.

Klein Goldewijk, K.: A historical land use data set for the Holocene; HYDE 3.2, *EGUGA*, pp. EPSC2016–1574, 2016.

565 Larsen, L. B., Vinther, B. M., Briffa, K. R., Melvin, T. M., Clausen, H. B., Jones, P. D., Siggaard-Andersen, M.-L., Hammer, C. U., Eronen, M., Grudd, H., et al.: New ice core evidence for a volcanic cause of the AD 536 dust veil, *Geophysical Research Letters*, 35, 2008.

Lehner, F., Born, A., Raible, C. C., and Stocker, T. F.: Amplified inception of European Little Ice Age by sea ice–ocean–atmosphere feedbacks, *Journal of climate*, 26, 7586–7602, 2013.

570 Liu, B., Liu, J., Ning, L., Sun, W., Yan, M., Zhao, C., Chen, K., and Wang, X.: The Role of Samalas Mega Volcanic Eruption in European Summer Hydroclimate Change, *Atmosphere*, 11, 1182, 2020.

Lücke, L. J., Hegerl, G. C., Schurer, A. P., and Wilson, R.: Effects of memory biases on variability of temperature reconstructions, *Journal of Climate*, 32, 8713–8731, 2019.

Ludescher, J., Bunde, A., Büntgen, U., and Schellnhuber, H. J.: Setting the tree-ring record straight, *Climate Dynamics*, 55, 3017–3024, 2020.

575 Luterbacher, J., Werner, J. P., Smerdon, J. E., Fernández-Donado, L., González-Rouco, F. J., Barriopedro, D., Ljungqvist, F. C., Büntgen, U., Zorita, E., Wagner, S., et al.: European summer temperatures since Roman times, *Environmental research letters*, 11, 024001, 2016.

Mann, M. E.: Little ice age, *Encyclopedia of global environmental change*, 1, 504–509, 2002.

580 Martrat, B., Eggleston, S., Abram, N., Bothe, O., Linderholm, H., McGregor, H., Neukom, R., Phipps, S., and St George, S.: The PAGES 2k Network: Understanding the climate of the Common Era (past 2000 years), in: *Geophysical Research Abstracts*, vol. 21, 2019.

Masson-Delmotte, V.: Coauthors, 2013: Information from paleoclimate archives, *Climate Change 2013: The Physical Science Basis*, 383, 464, 2013.

Mauritsen, T., Bader, J., Becker, T., Behrens, J., Bittner, M., Brokopf, R., Brovkin, V., Claussen, M., Crueger, T., Esch, M., et al.: Developments in the MPI-M Earth System Model version 1.2 (MPI-ESM1.2) and Its Response to Increasing CO₂, *Journal of Advances in Modeling Earth Systems*, 11, 998–1038, 2019.

585 Meinshausen, M., Vogel, E., Nauels, A., Lorbacher, K., Meinshausen, N., Etheridge, D., Fraser, P., Montzka, S., Rayner, P., Trudinger, C., et al.: Historical greenhouse gas concentrations, *Geoscientific Model Development Discussions*, 2016.

Miller, G. H., Geirsdóttir, Á., Zhong, Y., Larsen, D. J., Otto-Bliesner, B. L., Holland, M. M., Bailey, D. A., Refsnider, K. A., Lehman, S. J., Southon, J. R., et al.: Abrupt onset of the Little Ice Age triggered by volcanism and sustained by sea-ice/ocean feedbacks, *Geophysical Research Letters*, 39, 2012.

590 Moreno-Chamarro, E.: Climate and ocean variability during the last millennium in paleo-observations and Earth system model simulations, Ph.D. thesis, Universität Hamburg Hamburg, 2016.

Moreno-Chamarro, E., Zanchettin, D., Lohmann, K., Luterbacher, J., and Jungclaus, J. H.: Winter amplification of the European Little Ice Age cooling by the subpolar gyre, *Scientific Reports*, 7, 1–8, 2017.

Müller, M., Schwab, N., Schickhoff, U., Böhner, J., and Scholten, T.: Soil temperature and soil moisture patterns in a Himalayan alpine treeline ecotone, *Arctic, Antarctic, and Alpine Research*, 48, 501–521, 2016.

595 Myhre, G., Shindell, D., Bre'On, F.-M., Collins, W., Fuglestvedt, J., Huang, J., Koch, D., Lamarque, J.-F., Lee, D., Mendoza, B., Nakajima, T., Robock, A., Stephens, G., Takemura, T., and Zhang, H.: Anthropogenic and Natural Radiative Forcing, book section 8, p. 659–740, Cambridge University Press, Cambridge, United Kingdom and New York, NY, USA, <https://doi.org/10.1017/CBO9781107415324.018>, <http://www.climatechange2013.org>, 2013.

Neukom, R., Barboza, L. A., Erb, M. P., Shi, F., Emile-Geay, J., Evans, M. N., Franke, J., Kaufman, D. S., Lücke, L., Rehfeld, K., et al.: 600 Consistent multi-decadal variability in global temperature reconstructions and simulations over the Common Era, *Nature geoscience*, 12, 643, 2019.

Plunkett, G., Sigl, M., Schwaiger, H., Tomlinson, E., Toohey, M., McConnell, J. R., Pilcher, J. R., Hasegawa, T., and Siebe, C.: No evidence for tephra in Greenland from the historic eruption of Vesuvius in 79 CE: Implications for geochronology and paleoclimatology, *Climate of the Past Discussions*, pp. 1–37, 2021.

605 Pohlmann, H., Botzet, M., Latif, M., Roesch, A., Wild, M., and Tschuck, P.: Estimating the decadal predictability of a coupled AOGCM, *Journal of Climate*, 17, 4463–4472, 2004.

Polvani, L. M., Banerjee, A., and Schmidt, A.: Northern Hemisphere continental winter warming following the 1991 Mt. Pinatubo eruption: reconciling models and observations, *Atmospheric Chemistry and Physics*, 19, 6351–6366, 2019.

Rampino, M. R., Self, S., and Stothers, R. B.: Volcanic winters, *Annual Review of Earth and Planetary Sciences*, 16, 73–99, 1988.

610 Rao, M. P., Cook, B. I., Cook, E. R., D'Arrigo, R. D., Krusic, P. J., Anchukaitis, K. J., LeGrande, A. N., Buckley, B. M., Davi, N. K., Leland, C., et al.: European and Mediterranean hydroclimate responses to tropical volcanic forcing over the last millennium, *Geophysical research letters*, 44, 5104–5112, 2017.

Robock, A.: Volcanic eruptions and climate, *Reviews of geophysics*, 38, 191–219, 2000.

Robock, A. and Mao, J.: Winter warming from large volcanic eruptions, *Geophysical Research Letters*, 19, 2405–2408, 1992.

615 Schneider, D. P., Ammann, C. M., Otto-Bliesner, B. L., and Kaufman, D. S.: Climate response to large, high-latitude and low-latitude volcanic eruptions in the Community Climate System Model, *Journal of Geophysical Research: Atmospheres*, 114, 2009.

Schurer, A. P., Tett, S. F., and Hegerl, G. C.: Small influence of solar variability on climate over the past millennium, *Nature Geoscience*, 7, 104–108, 2014.

Sigl, M., McConnell, J. R., Layman, L., Maselli, O., McGwire, K., Pasteris, D., Dahl-Jensen, D., Steffensen, J. P., Vinther, B., Edwards, R., 620 et al.: A new bipolar ice core record of volcanism from WAIS Divide and NEEM and implications for climate forcing of the last 2000 years, *Journal of Geophysical Research: Atmospheres*, 118, 1151–1169, 2013.

Sigl, M., Winstrup, M., McConnell, J. R., Welten, K. C., Plunkett, G., Ludlow, F., Büntgen, U., Caffee, M., Chellman, N., Dahl-Jensen, D., et al.: Timing and climate forcing of volcanic eruptions for the past 2,500 years, *Nature*, 523, 543–549, 2015.

Solomina, O. N., Bradley, R. S., Jomelli, V., Geirsdottir, A., Kaufman, D. S., Koch, J., McKay, N. P., Masiokas, M., Miller, G., Nesje, A., 625 et al.: Glacier fluctuations during the past 2000 years, *Quaternary Science Reviews*, 149, 61–90, 2016.

Stenchikov, G., Robock, A., Ramaswamy, V., Schwarzkopf, M. D., Hamilton, K., and Ramachandran, S.: Arctic Oscillation response to the 1991 Mount Pinatubo eruption: Effects of volcanic aerosols and ozone depletion, *Journal of Geophysical Research: Atmospheres*, 107, ACL–28, 2002.

630 Stenchikov, G., Hamilton, K., Stouffer, R. J., Robock, A., Ramaswamy, V., Santer, B., and Graf, H.-F.: Arctic Oscillation response to volcanic eruptions in the IPCC AR4 climate models, *Journal of Geophysical Research: Atmospheres*, 111, 2006.

Stenchikov, G., Delworth, T. L., Ramaswamy, V., Stouffer, R. J., Wittenberg, A., and Zeng, F.: Volcanic signals in oceans, *Journal of Geophysical Research: Atmospheres*, 114, 2009.

Stevens, B., Giorgetta, M., Esch, M., Mauritsen, T., Crueger, T., Rast, S., Salzmann, M., Schmidt, H., Bader, J., Block, K., et al.: Atmospheric component of the MPI-M Earth system model: ECHAM6, *Journal of Advances in Modeling Earth Systems*, 5, 146–172, 2013.

635 Stevenson, S., Fasullo, J. T., Otto-Bliesner, B. L., Tomas, R. A., and Gao, C.: Role of eruption season in reconciling model and proxy responses to tropical volcanism, *Proceedings of the National Academy of Sciences*, 114, 1822–1826, 2017.

Stevenson, S., Overpeck, J. T., Fasullo, J., Coats, S., Parsons, L., Otto-Bliesner, B., Ault, T., Loope, G., and Cole, J.: Climate variability, volcanic forcing, and last millennium hydroclimate extremes, *Journal of Climate*, 31, 4309–4327, 2018.

Stothers, R. B.: Mystery cloud of AD 536, *Nature*, 307, 344–345, 1984.

640 Thompson, D. W. and Wallace, J. M.: The Arctic Oscillation signature in the wintertime geopotential height and temperature fields, *Geophysical research letters*, 25, 1297–1300, 1998.

Timmreck, C., Lorenz, S. J., Crowley, T. J., Kinne, S., Raddatz, T. J., Thomas, M. A., and Jungclaus, J. H.: Limited temperature response to the very large AD 1258 volcanic eruption, *Geophysical Research Letters*, 36, 2009.

Timmreck, C., Toohey, M., Zanchettin, D., Brönnimann, S., Lundstad, E., and Wilson, R.: The unidentified eruption of 1809: a climatic cold
645 case, *Climate of the Past*, 17, 1455–1482, 2021.

Toohey, M. and Sigl, M.: Volcanic stratospheric sulphur injections and aerosol optical depth from 500 BCE to 1900 CE, *Earth System Science Data*, 9, 809–831, 2017.

Toohey, M., Krüger, K., Niemeier, U., and Timmreck, C.: The influence of eruption season on the global aerosol evolution and radiative impact of tropical volcanic eruptions, *Atmospheric Chemistry and Physics*, 11, 12 351–12 367, 2011.

650 Toohey, M., Krüger, K., Bittner, M., Timmreck, C., and Schmidt, H.: The impact of volcanic aerosol on the Northern Hemisphere stratospheric polar vortex: mechanisms and sensitivity to forcing structure, *Atmospheric Chemistry and Physics*, 14, 13 063–13 079, 2014.

Toohey, M., Krüger, K., Sigl, M., Stordal, F., and Svensen, H.: Climatic and societal impacts of a volcanic double event at the dawn of the Middle Ages, *Climatic Change*, 136, 401–412, 2016a.

655 Toohey, M., Stevens, B., Schmidt, H., and Timmreck, C.: Easy Volcanic Aerosol (EVA v1. 0): an idealized forcing generator for climate simulations, *Geoscientific Model Development*, 9, 4049–4070, 2016b.

Toohey, M., Krüger, K., Schmidt, H., Timmreck, C., Sigl, M., Stoffel, M., and Wilson, R.: Disproportionately strong climate forcing from extratropical explosive volcanic eruptions, *Nature Geoscience*, 12, 100–107, 2019.

Trenberth, K. E. and Hoar, T. J.: El Niño and climate change, *Geophysical Research Letters*, 24, 3057–3060, 1997.

Usoskin, I., Hulot, G., Gallet, Y., Roth, R., Licht, A., Joos, F., Kovaltsov, G., Thébault, E., and Khokhlov, A.: Evidence for distinct modes of
660 solar activity, *Astronomy & Astrophysics*, 562, L10, 2014.

Van Loon, H. and Rogers, J. C.: The seesaw in winter temperatures between Greenland and northern Europe. Part I: General description, *Monthly Weather Review*, 106, 296–310, 1978.

Vieira, L. E. A., Solanki, S. K., Krivova, N. A., and Usoskin, I.: Evolution of the solar irradiance during the Holocene, *Astronomy & Astrophysics*, 531, A6, 2011.

665 Wegmann, M., Brönnimann, S., Bhend, J., Franke, J., Folini, D., Wild, M., and Luterbacher, J.: Volcanic influence on European summer precipitation through monsoons: possible cause for “Years without Summer”, *Journal of climate*, 27, 3683–3691, 2014.

Zanchettin, D., Timmreck, C., Graf, H.-F., Rubino, A., Lorenz, S., Lohmann, K., Krüger, K., and Jungclaus, J.: Bi-decadal variability excited in the coupled ocean–atmosphere system by strong tropical volcanic eruptions, *Climate Dynamics*, 39, 419–444, 2012.

Zanchettin, D., Bothe, O., Graf, H. F., Lorenz, S. J., Luterbacher, J., Timmreck, C., and Jungclaus, J. H.: Background conditions influence
670 the decadal climate response to strong volcanic eruptions, *Journal of Geophysical Research: Atmospheres*, 118, 4090–4106, 2013.

Zanchettin, D., Khodri, M., Timmreck, C., Toohey, M., Schmidt, A., Gerber, E. P., Hegerl, G., Robock, A., Pausata, F. S., Ball, W. T., et al.: The Model Intercomparison Project on the climatic response to Volcanic forcing (VolMIP): experimental design and forcing input data for CMIP6, *Geoscientific Model Development*, 9, 2701–2719, 2016.

Zhang, H., Yuan, N., Esper, J., Werner, J. P., Xoplaki, E., Büntgen, U., Treydte, K., and Luterbacher, J.: Modified climate with long term
675 memory in tree ring proxies, *Environmental Research Letters*, 10, 084 020, 2015.

Zhong, Y., Miller, G., Otto-Bliesner, B., Holland, M., Bailey, D., Schneider, D., and Geirsdottir, A.: Centennial-scale climate change from decadally-paced explosive volcanism: a coupled sea ice-ocean mechanism, *Climate Dynamics*, 37, 2373–2387, 2011.

680 **Appendix A - Model - tree-ring, and multi-proxy reconstruction comparison**

Most temperature reconstruction data sets go back to about 1200 CE, and the further back in time, the fewer proxy records remain, and the more uncertainties they contain (Masson-Delmotte, 2013; Esper et al., 2018; Neukom et al., 2019). The main proxy type that remains to reconstruct the temperatures in the Northern Hemisphere (and especially mid-high latitudes, Europe) are tree rings (Neukom et al., 2019), and they are often used to reconstruct the temperature in especially Europe (Luterbacher 685 et al., 2016). Other reconstructions available consist of a mix of proxies with a more limited dating precision, which leads to a reduction of the amplitude of the signals (Sigl et al., 2015; Büntgen et al., 2020; Plunkett et al., 2021). Only $\sim 25\%$ of the proxies available for our study period have annual dating precision (Neukom et al., 2019).

690 The data sets used for the individual tree-ring sites are from Northern Scandinavia (N-Scan) (Esper et al., 2012b, a), from the Alps and Altai (Büntgen et al., 2016) and from Europe (Luterbacher et al., 2016) (Table 2). We have also carried out a comparison for other individual sites in the NH (see tree-ring sites in Figure A1), but due to a high internal variability the volcanic signal does not stand out for the model simulated temperatures. We could therefore not use these sites for a model - tree-ring comparison.

Table 2. Overview of tree-ring/proxy locations and type (MXD: maximum latewood density; TRW: tree ring width) used in this individual comparison. For the proxy reconstructions from Luterbacher et al. (2016) and Neukom et al. (2019) the method used is composite plus scaling (CPS).

Location name	Coordinates	Type of data	Reference
N-Scan	66° - 70°N, 19° - 29°E	MXD	Esper et al. (2012b, a)
Alps	46°N, 12.5°E	TRW	Büntgen et al. (2016)
Altai	50°N, 87.5°E	TRW	Büntgen et al. (2016)
Europe	35°- 70°N, -25°- 40°E	TRW and MXD	Luterbacher et al. (2016)
NH	0°- 90°N, -180°- 180°E	mixed proxies	Neukom et al. (2019)

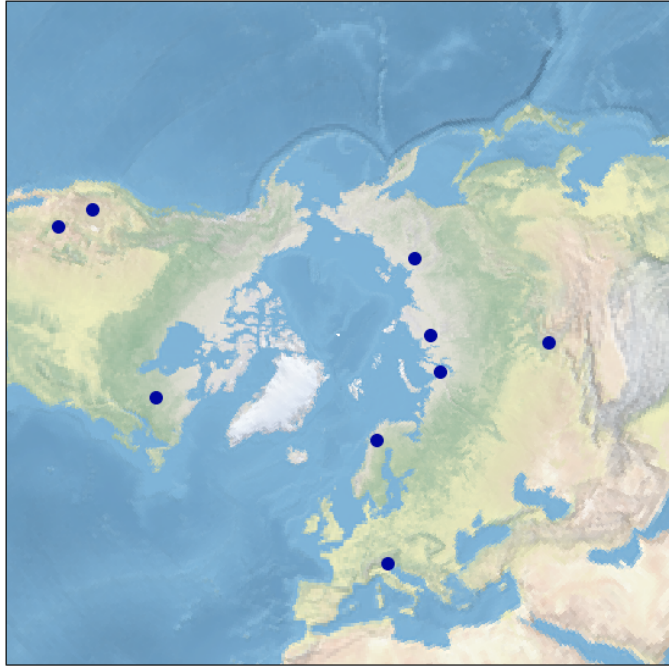


Figure A1. Locations of the tree-ring sites used in this study from Büntgen et al. (2021).

695 The NH tree-ring ensemble reconstruction (Büntgen et al., 2021) consists only of tree ring width (TRW). TRW has biological
 memory and gives a lagged and smoothed response to volcanic eruptions. In contrast, MXD is based on cell density, which
 represents the volcanic climate response well (Esper et al., 2015; Zhu et al., 2020). MXD gives a better representation of surface
 temperature anomalies (Anchukaitis et al., 2012; Esper et al., 2015; Zhu et al., 2020; Ludescher et al., 2020) and is therefore
 the preferred target for our model comparison if available. However, as MXD data is sparse during the first millennium, the
 700 tree ring proxies consist mainly of TRW data. Only the data from N-Scan (Esper et al., 2012b, a) consists of MXD.

The used tree-ring data are provided as temperature anomalies with respect to 1961-1990 CE. To use the same reference
 periods for the model and tree-ring data, we recalculate the tree-ring reconstructed temperature anomalies with respect to 0-
 1850 CE. For the model-tree-ring comparison a land mask was applied to the model 2m air temperature analyzing the NH
 extratropics between 40° and 75°N. The tree-ring data sets used here capture the boreal summer temperature during June, July
 705 and August (JJA) (Büntgen et al., 2016) and were therefore compared to JJA 2m air temperatures from the model.

Figure A2a shows the model - tree-ring comparison for N-Scan. Just as for the NH, the variability of the reconstructed
 temperatures fall within the spread of the model simulations. The peak cooling of the 536 and 540 CE eruptions agrees very
 well both in timing and in maximum cooling. This could be because the tree-ring data for N-Scan consists of MXD data, so
 710 there is less time lag and smoothing in the signal (Esper et al., 2015).

The tree-ring reconstructions for the Alps and Altai (Fig. A2b and c) show more discrepancies compared to the N-Scan site or the NH tree-ring ensemble reconstruction. The tree-ring temperatures still fall within the variability of the model simulations, but the maximum of the cooling for the four large eruptions does not always agree so well. For the Alps, the recovery time after the 536/540 CE eruptions is longer for the tree-ring temperatures than for the model, showing a lag, as for the NH compilation.

715 For the Altai, the cooling in the tree-ring reconstructions after the 536/540 CE eruptions lasts even longer until \sim 660 CE, revealing a large discrepancy between the model temperature and the reconstructed temperature for this site.

For Europe, the model and proxy data (Luterbacher et al., 2016) agree well. The proxy reconstruction falls within the spread of the model ensemble (Fig. A2d). As for the comparison with Büntgen et al. (2021), the peak cooling is less for the reconstructions, and there is a lag in the proxy data after 540 CE.

720 To illustrate the reduction in amplitude of the signals, we compared the Pages2k multi-proxy reconstruction (Neukom et al., 2019) to the simulated NH annual mean near surface temperature (Fig. A3). The proxy data agrees well for the recovery period after the 536/540 CE double eruption, and from \sim 650 CE - 675 CE, but the reconstructions show a weaker cooling following the volcanic eruptions, and for the 574 CE eruption the reconstruction does not show a signal at all.

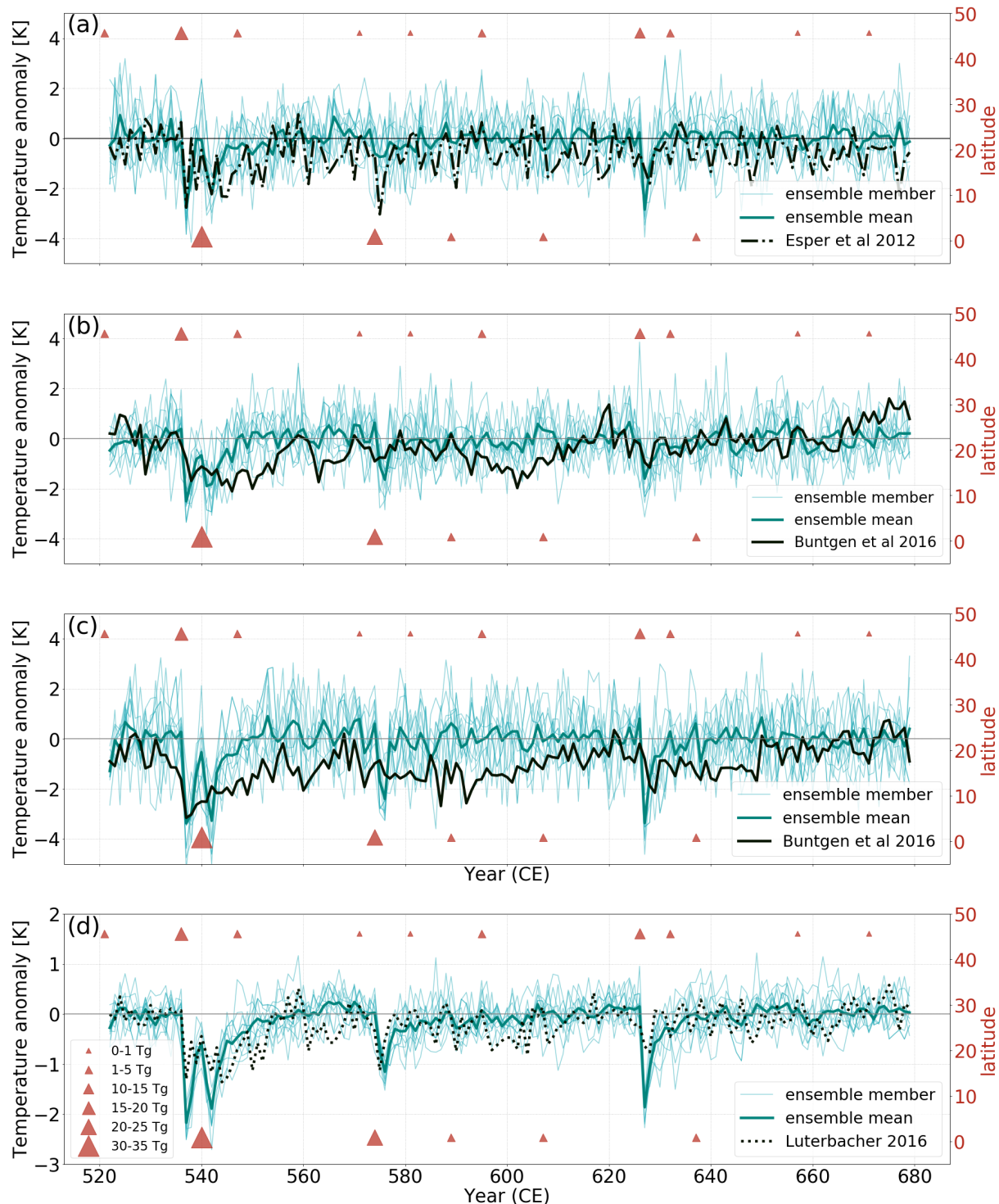


Figure A2. Model - tree-ring comparison for a) Northern Scandinavia (N-Scan) (Esper et al., 2012b), b) the Alps and c) the Altai (Büntgen et al., 2016) and Europe ((Luterbacher et al., 2016). Mean anomalies are calculated for the 0-1850 CE reference period. The red triangles represent the volcanic eruptions from the model forcing according to their latitude (tropical or NH extratropical), and the size of the triangle corresponds to the estimated range of sulphur [Tg S] injected into the stratosphere (Toohey and Sigl, 2017).

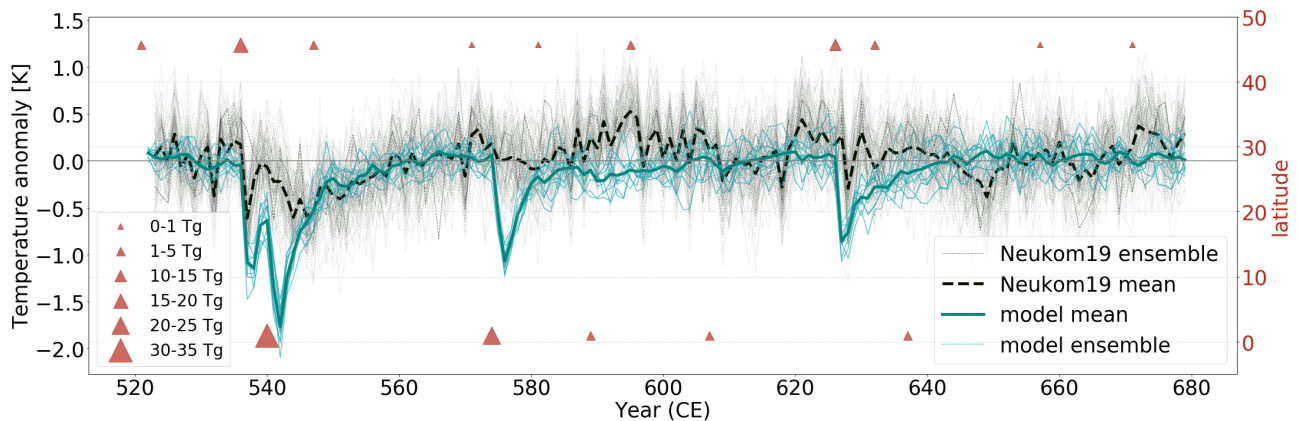


Figure A3. Model - proxy reconstruction comparison for the entire Northern Hemisphere with PAGES2k data (Neukom et al., 2019). Mean anomalies are calculated for the 0-1850 CE reference period. The red triangles represent the volcanic eruptions from the model forcing according to their latitude (tropical or NH extratropical), and the size of the triangle corresponds to the estimated range of sulphur [Tg S] injected into the stratosphere (Toohey and Sigl, 2017).

Appendix B - NAO

725 The climate in the North Atlantic and Europe is often indicated by the state of the North Atlantic Oscillation (NAO). The NAO describes variations of the sea level pressure difference between Iceland and the Azores, leading to wind patterns carrying warm moist air to Northern Europe (positive NAO phase), or dry cold air (negative NAO phase). For this study, we calculated the NAO index using the method from Hurrell (1995). The NAO index is calculated by taking the first principle component of the SLP anomalies for the area 90°W to 40°E , 20°N to 80°N . The obtained time series then indicates whether the NAO is in
 730 a positive or negative phase, where a positive NAO corresponds to relatively warmer and wetter conditions over Scandinavia, and the negative phase corresponding to the opposite (Hurrell, 1995). See Figure A4 and Table A1.

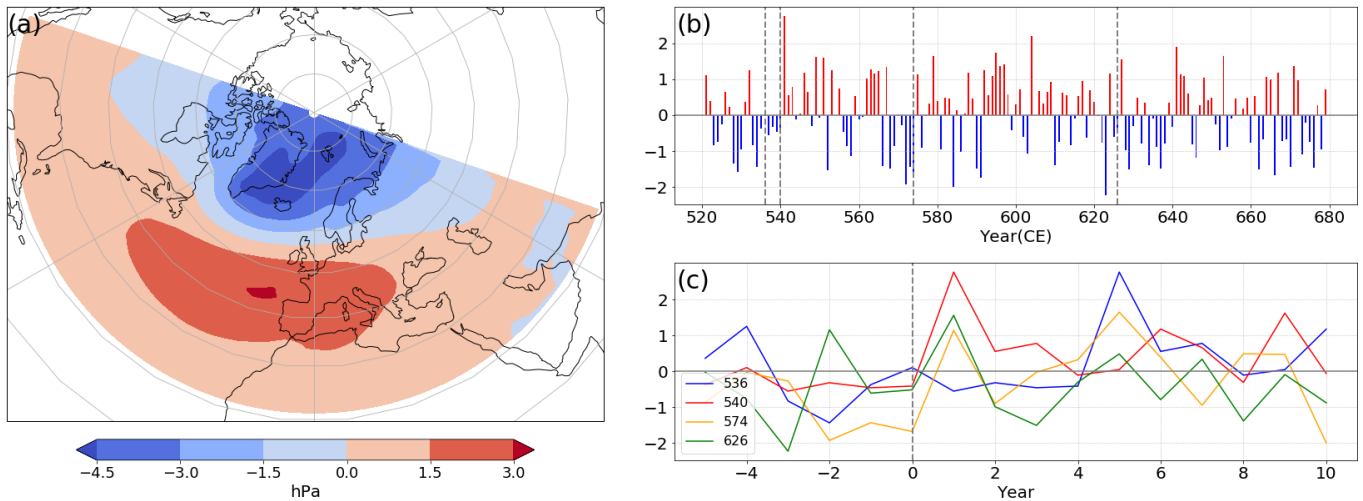


Figure A4. NAO DJF for (a) the climatological NAO signal for 0-1850 CE past2k "run 0", and the response as (b) a time series of the ensemble mean NAO index and (c) an epoch analysis of the NAO index for the four large eruptions during 520 to 680 CE. The eruption years are indicated with a dashed vertical black line in (b). DJF year 0 corresponds to December of the year before the eruption, and January to February of the year of the eruption.

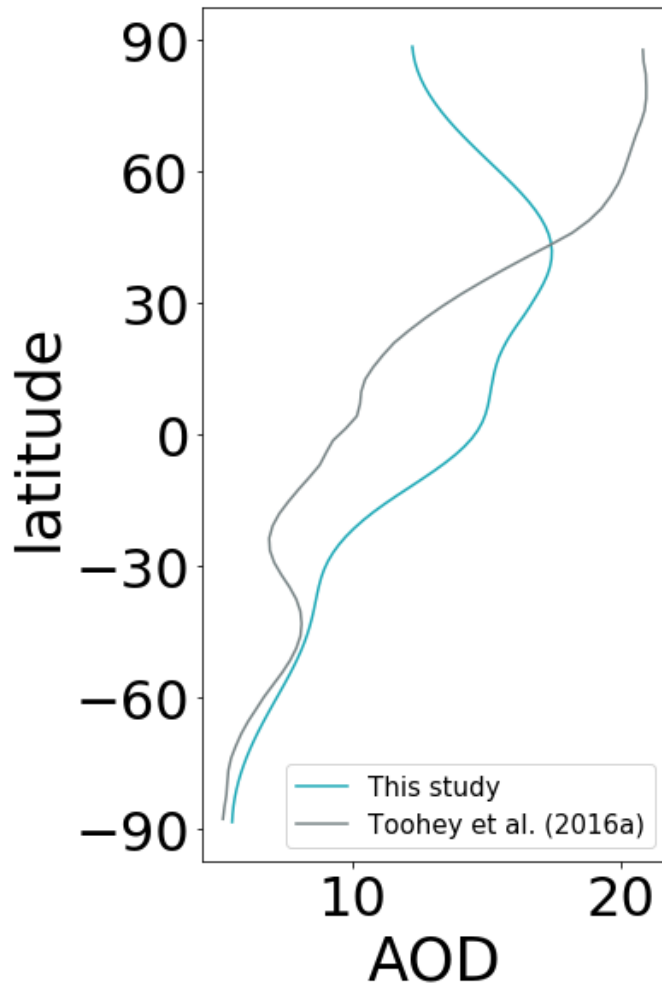


Figure A5. Comparison for accumulated AOD for 536-550 CE for the volcanic forcing from this study (eVolv2k(EVA), Toohey and Sigl, 2017) and from Toohey et al. (2016a) (their Figure 2d, based on MAECHAM-HAM).

Appendix C - Climate indices

Zanchettin et al. (2013) identified the importance of background conditions for ensemble-based numerical studies of large volcanic eruptions as they have an impact on the mechanisms involved in the post-eruption decadal evolution. To determine the background conditions, i.e., the initial climate state of our ensemble members and to address the climate variability during 520 CE to 680 CE several relevant climate indices were calculated.

North Atlantic

Since the focus of this study is on Europe, the initial state of the North Atlantic (NA) ocean and sea ice was calculated. In Table 740 A1, the Atlantic meridional overturning circulation (AMOC), the strength of the barotropic streamfunction (BTS) and the SST for the subpolar gyre are given; Fig. A6 displays the time series of these quantities for the 520-680 CE and past2k runs. The AMOC is defined as the maximum in the mass streamfunction, which occurs between 35° and 45°N and 800 m to 1200 m depth in the MPI-ESM past2k run 0 climatology (0-1850 CE mean). The column integrated BTS can be used as a measure for the strength of the subpolar gyre, which is the horizontal flow south of Greenland with an anticlockwise rotation. The subpolar 745 gyre in the climatology resides between 50°N and 65°N and 20° to 60°W, so we take this area as a measure for the state of the BTS and for the SST. From Table A1 and Figure A6 it becomes clear that the initial ocean and sea ice state before 536 CE covers mean North Atlantic conditions of the past 1850 years. See Figure A6 and Table A1.

ENSO

The El Niño Southern Oscillation (ENSO) index was calculated using the Niño 3.4 index, as described by Trenberth and Hoar 750 (1997). The sea surface temperature (SST) anomaly was calculated for the box 5°S - 5°N and 120°-170°W. If the 5-month running mean exceeds 0.4°C for 6 months or more, the ENSO state is defined as an El Niño (Trenberth and Hoar, 1997). La Niña is defined in the same way, but for -0.4°C instead.

Figure A6 and Table A1 give an overview of the ENSO conditions before the four large volcanic eruptions. The spread in the ensembles cover a wide range of different ENSO states at the beginning of the transient runs.

755

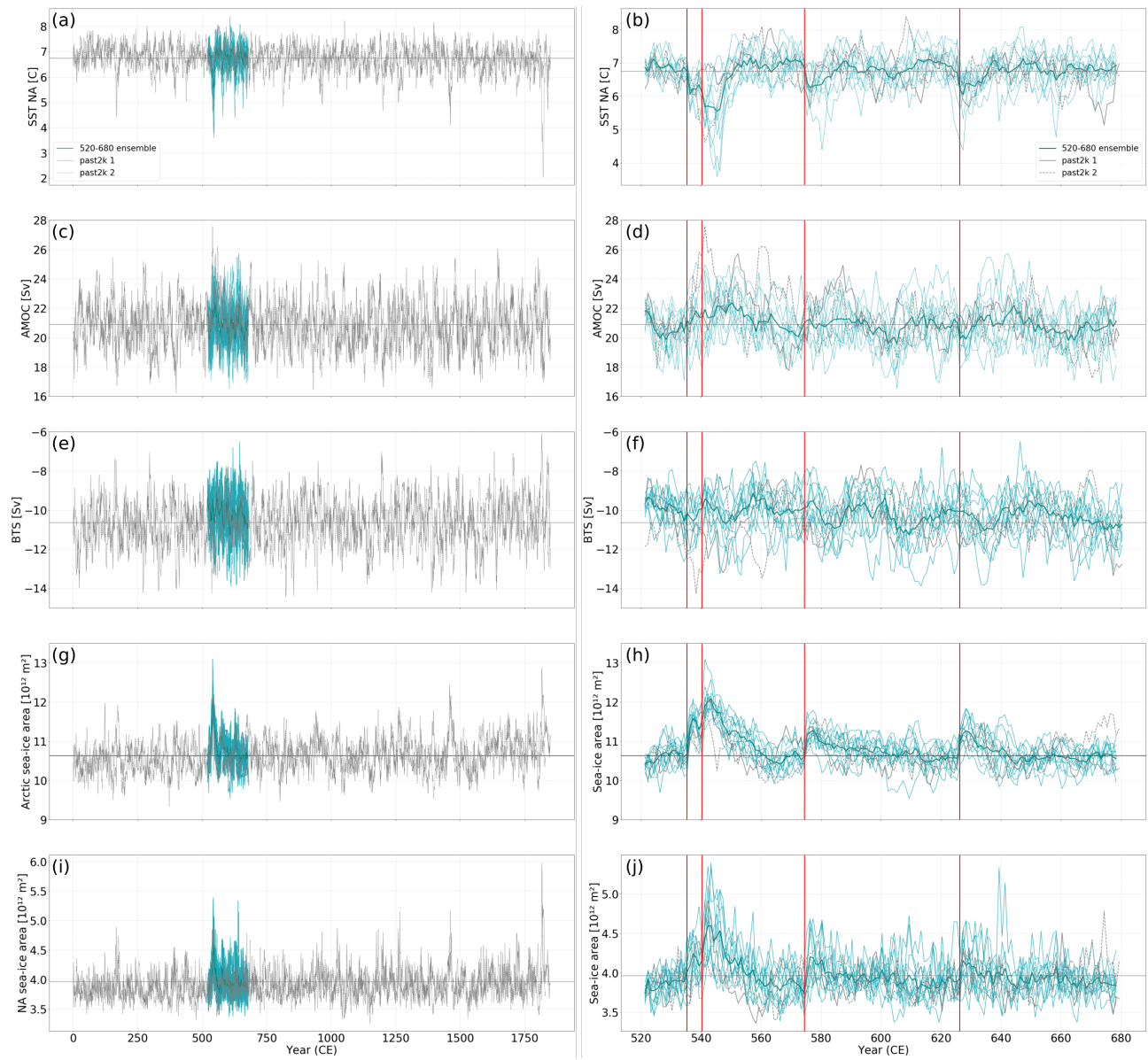


Figure A6. Time series for a/b) NA SST, c/d) AMOC, e/f) BTS, g/h) Arctic sea-ice area and i/j) NA sea-ice area for 0-1850 CE (left panels) and 521-680 CE (right panels). The red lines indicate the large volcanic eruptions in the study period, and the straight gray line is the mean of the past2k "run 0".

Table A1. Initial ocean and sea ice conditions. Mean and [range] of all ensemble members for the AMOC, subpolar gyre BTS and SST, NA March sea ice area, and ENSO states (Niño3.4 index) before the four large eruptions. *For all quantities the mean of the previous year of the eruptions are calculated except for the Niño3.4 index, where the 5 month rolling mean (ASOND) of the previous year was taken.

Variable* / Eruption	536 CE (extratropical)	540 CE (tropical)	574 CE (tropical)	626 CE (extratropical)
AMOC [Sv]	20.96 [19.16, 21.77]	21.81 [18.76, 25.82]	20.35 [18.53, 24.25]	20.92 [19.73, 22.31]
Subpolar gyre BTS [Sv]	-10.35 [-8.75, -12.26]	-10.09 [-8.79, -11.29]	-10.16 [-8.71, -11.41]	-10.22 [-8.71, -12.76]
Sub-Polar Gyre SST [°C]	6.69 [6.22, 7.16]	6.28 [5.09, 6.82]	6.97 [6.22, 7.69]	6.65 [4.95, 7.59]
NA March sea-ice area [10 ¹² m ²]	3.95 [3.57, 4.48]	4.10 [3.68, 4.84]	3.86 [3.54, 4.23]	3.88 [3.65, 4.65]
Niño3.4 index	2 neutral 5 La Niña 5 El Niño	1 neutral 10 La Niña 1 El Niño	7 neutral 1 La Niña 4 El Niño	6 neutral 4 La Niña 2 El Niño